Composites: Part A 56 (2014) 8–26

Contents lists available at ScienceDirect

Composites: Part A

journal homepage: www.elsevier.com/locate/compositesa

Shear characterisation of uni-directional fibre reinforced thermoplastic melts by means of torsion

S.P. Haanappel [a,*], R. Akkerman [a,b]

[a] ThermoPlastic composites Research Center (TPRC), P.O. Box 770, 7500AT Enschede, The Netherlands
[b] Faculty of Engineering Technology, Chair of Production Technology, University of Twente, P.O. Box 217, 7500AE Enschede, The Netherlands

ARTICLE INFO

Article history:
Received 4 February 2013
Received in revised form 8 September 2013
Accepted 14 September 2013
Available online 24 September 2013

Keywords:
A. Fibres
A. Thermoplastic resin
B. Rheological properties
E. Forming

ABSTRACT

Intra-ply shear appears during the forming process of hot thermoplastic laminates with a uni-directional fibre reinforcement. This paper proposes a torsion bar test to characterise the longitudinal shear mechanism, which can be performed with a standard rheometer. Sensitivity analyses showed that most reliable shear property measurements can be obtained by using torsion bar specimens with a close to square cross section. The method is implemented in practise and critically evaluated. Storage and loss moduli were determined for carbon UD/PEEK specimens at high temperatures. Non-linear material behaviour was found for relatively small shear strains. The linear regime was focussed on subsequently, where the characteristics were found to be similar to that of a visco-elastic solid or weak gel, confirmed by a dominant storage modulus and a weak frequency dependency. Future work is recommended to be focussed on the large strain regime, for which this paper provides a found basis.

1. Introduction

Thermoforming of fibre reinforced thermoplastic laminates is ideally suited for the production of thin-walled products with complex curvatures. Nevertheless, process induced defects appear frequently, such as the wrinkling shown in Fig. 1. Better anticipation on such defects facilitates the tooling design process by which significant lead-time reductions can be achieved. Analyses of uni-directional (UD) carbon fibre reinforced thermoplastics have been reported for decades already [1]. Nevertheless, textile reinforced thermoplastics or fabrics were favoured due to their ease of forming onto complex shaped moulds. However, it is believed that the high directional strength and stiffness properties of UD material can be fully exploited with the aid of sophisticated deposition tooling, such as tape placement robots [2]. A subsequent forming operation of so-called tailored blanks can be carried out. These possibilities revive the interest in UD material for forming applications again.

The forming process of UD reinforced thermoplastic laminates involves several deformation processes which were previously categorised by Cogswell [3,4]. Inter-ply slip is identified as the mechanism where individual plies slide relatively to each other, implying a discontinuous displacement field over the laminate thickness. Laminates with good consolidation quality and equally oriented plies show a more continuous intra-ply shearing deformation [5]. Intra-ply shear refers to the shearing process within a UD reinforced ply. Two intra-ply shearing deformations are usually distinguished [6]. The first considers parallel sliding of individual fibre filaments, which is indicated as axial or longitudinal intra-ply shearing. The second is transverse intra-ply shearing, which is the relative movement of the fibres normal to the fibre directions. These mechanisms are schematically shown in Fig. 2. They appear simultaneously when forming a doubly curved part, which in addition induces (out-of-plane) bending of the laminate. The final product shape will be determined by the complex interaction of intra-ply shear, inter-ply slippage, and bending.

The wrinkles in Fig. 1 can be avoided by ensuring that the longitudinal shearing mechanism is more pronounced. The transverse shear mechanism is of less importance, when solving such forming issues. In order to predict the defects in the early product design phase, it is important to have a proper description of the longitudinal shearing mechanism. An overview of available shear characterisation tests is presented, after supplying some background about the modelling of anisotropic media and the basis of Linear Visco-Elasticity (LVE) theory [7]. The need for another shear characterisation tests is explained next, followed by the introduction of the torsion bar method (Fig. 3). The kinematics of a torsionally loaded rectangular bar will be analysed resulting in guidelines for specimen geometry. Experiments are subsequently presented for specimens that consist of AS4 carbon fibres with a polyetheretherketone (PEEK) matrix. This pre-preg material is shown in Fig. 4. The micrograph gives an impression of the fibrous structure. Specimen responses are analysed in detail in order to explore the conditions that lead to linear and non-linear material behaviour. The first

* Corresponding author.
E-mail address: s.p.haanappel@utwente.nl (S.P. Haanappel).

1359-835X/$ - see front matter © 2013 Elsevier Ltd. All rights reserved.
http://dx.doi.org/10.1016/j.compositesa.2013.09.007

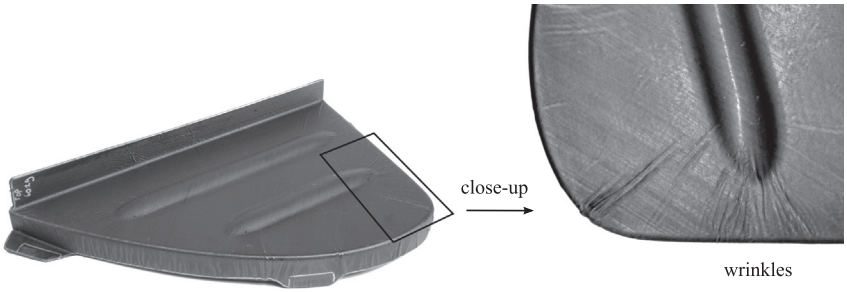

Fig. 1. Process induced defects.

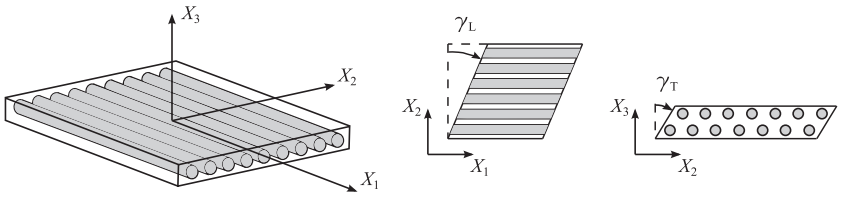

Fig. 2. Left: definition of the coordinate system with respect to the fibre direction. Centre: axial or longitudinal intra-ply shearing. Right: transverse intra-ply shearing.

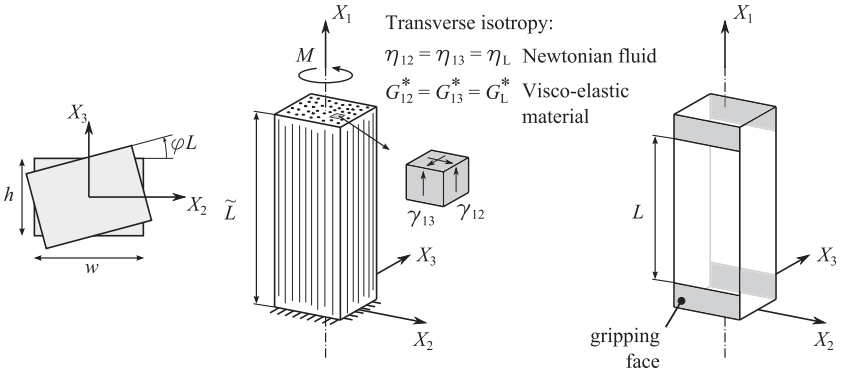

Fig. 3. Conceptual design of the torsion bar specimen. Left: cross sectional geometry. Centre: fibre reinforced rectangular bar. Torsional loading invokes longitudinal shear mechanisms as indicated by the elementary cube. Right: grey areas represent the aimed gripping faces to conduct torsional loads in practise.

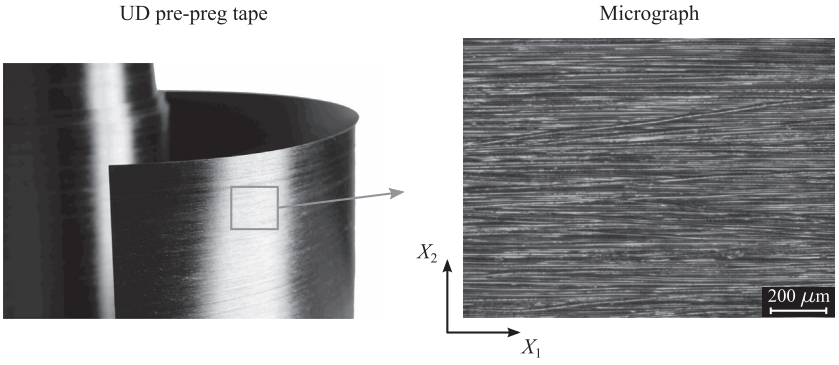

Fig. 4. Carbon UD/PEEK pre-preg tape and a micrograph giving an impression of its micro-structure.

implementation step of this method in practise involves the linear material behaviour during oscillatory small strain measurements. Transient responses are of interest for stamp forming applications and thus a translation from the dynamic moduli to the relaxation modulus will be obtained. Finally, recommendations are given for further development of the introduced torsion bar method.

2. Modelling of anisotropic media

Two approaches can be found in the literature to describe transversely isotropic viscous fluids. They differ in the assumption of the material form, which consists of continuously or discontinuously collimated fibres [8].

2.1. Ideal fibre reinforced Newtonian fluid model

The first approach assumes continuously collimated fibres, which is most representative for the material used in this research. An anisotropic elastic model that accounts for large deformations and the dominating presence of a single family of inextensible fibres was initially developed by Spencer [9]. The incompressibility assumption led to the addition of an arbitrary hydrostatic pressure term p. This model was adopted by Rogers [10] to account for visco-elastic fluids. The special case of a linear viscous fluid was obtained, which was referred to as the Ideal Fibre Reinforced Newtonian fluid Model (IFRM). The Cauchy stress $\boldsymbol{\sigma}$ is expressed as:

$$\boldsymbol{\sigma} = -p\boldsymbol{I} + T\boldsymbol{a}\boldsymbol{a} + 2\eta_T\boldsymbol{D} + 2(\eta_L - \eta_T)(\boldsymbol{a}\boldsymbol{a}\cdot\boldsymbol{D} + \boldsymbol{D}\cdot\boldsymbol{a}\boldsymbol{a}) \tag{1}$$

where T is the fibre stress, $\boldsymbol{a}$ is the vector that represents the fibre direction in the deformed state, $\boldsymbol{D}$ is the rate of deformation tensor, and $\boldsymbol{I}$ is the second order unit tensor. The parameters η_T and η_L represent the transverse and axial or longitudinal viscosity of the uni-directional ply respectively. These are related to the shearing mechanisms of a fibre reinforced viscous fluid, as shown in Fig. 2. If the fibre direction coincides with the X_1-axis, the matrix representation of this constitutive model can be written as:

$$\begin{bmatrix} \sigma_{11}+p-T \\ \sigma_{22}+p \\ \sigma_{33}+p \\ \sigma_{23} \\ \sigma_{31} \\ \sigma_{12} \end{bmatrix} = \begin{bmatrix} 4\eta_L-2\eta_T & & & & & \\ & 2\eta_T & & & & \\ & & 2\eta_T & & & \\ & & & \eta_T & & \\ & & & & \eta_L & \\ & & & & & \eta_L \end{bmatrix} \begin{bmatrix} \dot{\epsilon}_{11} \\ \dot{\epsilon}_{22} \\ \dot{\epsilon}_{33} \\ \dot{\gamma}_{23} \\ \dot{\gamma}_{31} \\ \dot{\gamma}_{12} \end{bmatrix} \tag{2}$$

where, strictly speaking, the first row is arbitrary as the material is inextensible in the fibre direction: $\dot{\epsilon}_{11} = 0$.

2.2. Linear viscous transversely isotropic fluid

The second approach assumes discontinuously collimated fibres with typical lengths of 100 mm. Starting with the linear description of a fully anisotropic fluid, Beaussart et al. [11] reduced the 21 independent material parameters to three by assuming incompressibility and transverse isotropy. In case the fibre direction is parallel to the X_1-axis, the resulting matrix formulation in compliance form then reads:

$$\begin{bmatrix} \dot{\epsilon}_{11} \\ \dot{\epsilon}_{22} \\ \dot{\epsilon}_{33} \\ \dot{\gamma}_{23} \\ \dot{\gamma}_{31} \\ \dot{\gamma}_{12} \end{bmatrix} = \begin{bmatrix} \beta_{11} & -\beta_{11}/2 & -\beta_{11}/2 & & & \\ -\beta_{11}/2 & \beta_{22} & \beta_{11}/2-\beta_{22} & & & \\ -\beta_{11}/2 & \beta_{11}/2-\beta_{22} & \beta_{22} & & & \\ & & & 4\beta_{22}-\beta_{11} & & \\ & & & & \beta_{66} & \\ & & & & & \beta_{66} \end{bmatrix} \begin{bmatrix} \sigma_{11}+p \\ \sigma_{22}+p \\ \sigma_{33}+p \\ \sigma_{23} \\ \sigma_{31} \\ \sigma_{12} \end{bmatrix} \tag{3}$$

where p is the hydrostatic pressure. The terms σ_{ij} are the stress, $\dot{\epsilon}_{ij}$ the extensional strain rate, and $\dot{\gamma}_{ij}$ the shear rate components. The parameters β_{ij} are the reciprocals of viscosities (fluidities). The indices i and j correspond to the axes defined in Fig. 2. Three independent viscosity parameters were defined:

$$\eta_{11} = \beta_{11}^{-1} \quad \eta_{22} = \eta_{33} = \beta_{22}^{-1} \quad \eta_{23} = (4\beta_{22} - \beta_{11})^{-1} \quad \eta_{12} = \eta_{13} = \beta_{66}^{-1} \tag{4}$$

and represent the axial elongational, transverse elongational, transverse shearing, and in-plane shearing viscosity, respectively. Analytical derivations for these viscosities were given by for example Pipes et al. [8] and Christensen [12].

The difference between the relations (3) and (2) is the result of the different material form assumption, namely the extensibility condition in the fibre direction. It can be shown that Eq. (3) simplifies to the IFRM formulation in Eq. (2) when the inextensibility constraint is imposed. When the deviatoric stresses and strain rates are considered, the singular system in (3) can be inverted by using the constraints of incompressibility. The condition of inextensibility:

$$\dot{\epsilon}_{11} = 0 \tag{5}$$

$$\dot{\epsilon}_{33} = -\dot{\epsilon}_{22} \tag{6}$$

can then be used to eliminate the off-diagonal terms, leading to:

$$\begin{bmatrix} \sigma_{11}+p \\ \sigma_{22}+p \\ \sigma_{33}+p \\ \sigma_{23} \\ \sigma_{31} \\ \sigma_{12} \end{bmatrix} = \begin{bmatrix} \frac{2}{3\beta_{11}} & & & & & \\ & \frac{2}{4\beta_{22}-\beta_{11}} & & & & \\ & & \frac{2}{4\beta_{22}-\beta_{11}} & & & \\ & & & \frac{1}{4\beta_{22}-\beta_{11}} & & \\ & & & & \frac{1}{\beta_{66}} & \\ & & & & & \frac{1}{\beta_{66}} \end{bmatrix} \begin{bmatrix} \dot{\epsilon}_{11} \\ \dot{\epsilon}_{22} \\ \dot{\epsilon}_{33} \\ \dot{\gamma}_{23} \\ \dot{\gamma}_{31} \\ \dot{\gamma}_{12} \end{bmatrix} \tag{7}$$

where we again note that the first row is an arbitrary statement. Comparison of Eq. (7) with the IFRM relation in (2) confirms that:

$$\eta_L = \frac{1}{\beta_{66}} = \eta_{12} = \eta_{13} \tag{8}$$

$$\eta_T = \frac{1}{4\beta_{22} - \beta_{11}} = \eta_{23} \tag{9}$$

2.3. Rheometry

Deformation of a polymer melt is usually associated with mechanisms such as viscous dissipation and storage of elastic energy. Its constitutive behaviour can be described with the well-known Linear Visco-Elasticity (LVE) theory [7] for small strains. To measure the response of a material, it is favourable to apply a simple deformation such that it can be regarded as a 1D situation. Simple shearing invokes only one off-diagonal pair of the strain tensor components:

$$\gamma_{ij} = \begin{bmatrix} 0 & \gamma_{12} & 0 \\ \gamma_{21} & 0 & 0 \\ 0 & 0 & 0 \end{bmatrix} \tag{10}$$

Dynamic mechanical testing is often applied to measure material responses at short time scales. A sinusoidal deformation with angular frequency ω and strain amplitude γ_{12}^0 can be applied:

$$\gamma_{12}(t) = \gamma_{12}^0 \sin(\omega t) \tag{11}$$

For linear material behaviour, the stress response is also sinusoidal:

$$\sigma_{12}(t) = \sigma_{12}^0 \sin(\omega t + \delta) \tag{12}$$

which runs out-of-phase with phase angle δ when the material behaves visco-elastically, as shown in Fig. 5. The linear visco-elastic material properties are represented by the storage and loss moduli, respectively [7]:

$$G' = \frac{\sigma_{120}}{\gamma_{120}}\cos\delta \quad G'' = \frac{\sigma_{120}}{\gamma_{120}}\sin\delta \tag{13}$$

The complex shear modulus is defined as:

$$G^* = G' + iG'' \tag{14}$$

where i denotes the imaginary number. The damping of the material is defined as:

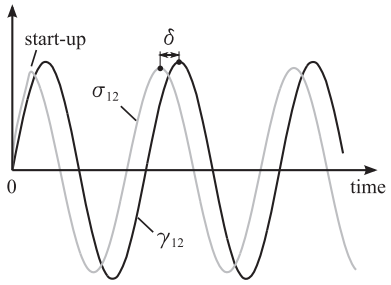

Fig. 5. The stress response of a visco-elastic material that is subjected to a sinusoidally applied strain.

$$\tan\delta = \frac{G''}{G'} \tag{15}$$

The dynamic and out-of-phase viscosities are respectively related to the loss and storage modulus through the angular frequency:

$$\eta' = \frac{G''}{\omega} \quad \eta'' = \frac{G'}{\omega} \tag{16}$$

The complex viscosity is defined as:

$$\eta^* = \eta' - i\eta'' \tag{17}$$

The LVE theory assumes the material under consideration exists as a continuum, implying that the material and its mechanical properties are continuously distributed. A composite material in melt may deviate from this criterion. Therefore, the dynamic properties are regarded as the 'apparent' properties in the remainder of the paper.

3. Review of shear characterisation methods

The development of intra-ply shear characterisation tests originates from the urge to quantify the strength and stiffness of structural components. Different tests were developed to test composite laminates in their solidified state, which were summarised in several review papers [13,14]. One can think of two and three rail shear tests, off-axis tests and picture frame tests which are all standardised by for example the ASTM organisation, not necessarily intended for composite material testing. Shear characterisation methods by means of torsional loadings have also been developed. These comprise prismatic rods with a rectangular cross section and thin-walled tubes.

Other methods, some of them probably inspired by above mentioned methods for solidified materials, have been developed to characterise composite materials in their flexible state as they are used in forming processes. An overview of methods was given by Harrison and Clifford [15]. A comparison between the measured material parameters showed deviations up to two orders of magnitude. Earlier work [16] showed that forming predictions are sensitive to the observed deviations. Accurate characterisation data is therefore required.

Tables 1 and 2 summarise previously developed methods to characterise the longitudinal shearing mechanism of fibre reinforced polymer melts. The methods differ in many aspects, for example the specimen size, geometry, and the type of load introduction, which can be done in a transient or dynamic manner. For the transient experiments, different strain rates were reported and shear strain magnitudes vary from small and linear up to large and non-linear. Dynamic experiments were carried out at different strain amplitudes and frequency ranges, where their translation to shear rates in the transient domain is not straightforward.

Groves et al. [17–19] introduced a characterisation test where laminates are positioned between two parallel plate fixtures (Fig. 6(a)). The first publication [17] dealt with cross plied and UD laminates covering the whole platen surface. In this way, longitudinal and transverse shearing deformations are applied simultaneously. A shear deformation is applied by rotating one of the plates. Both oscillating shear and steady shear deformations were applied. Results for both type of laminates were similar and the response was said to be isotropic. A later publication [19] showed the results that were obtained by positioning two square laminates in an off-centred manner, such that both shearing modes could be characterised separately. The measured parameters were represented by using the LVE theory and the use of the well-known dynamic Voigt parameters G'' and η''. Easier interpretation of the results was obtained by using the dynamic Maxwell parameters [20].

Instead of a rotating fixture, Scobbo and Nakajima [21,22] induced an oscillating shear deformation by means of a translational motion of a plate-type fixture (Fig. 6(b)). The testing material is in contact with both sides of this dynamic plate, while fixed platens are in contact with the other sides of the specimens. Also here, results were presented in terms of the dynamic Voigt parameters by assuming the LVE theory.

Table 1
Longitudinal shear characterisation methods. (?) means that information was not explicitly given.

Ref.	Fig. 6	Built-in device	Fixture type	Fixture movement	Movement type	Specimen dimension [mm] (in-plane dim. × thickness)
Groves [17]	(a)	Rheometer	Plate–plate	Rotation	Oscillating and Transient	≈Ø25×?
Scobbo and Nakajima [21,22]	(b)	Modified Mechanical Energy Resolver (MER)	Plate–plate–plate	Translation	Oscillating	14×14×3
Wheeler and Jones [23]	(c)	Custom-built Linear oscillator	Plate–plate	Translation	Oscillating	10×10×0.5
Groves et al. [19]	(a)	Rheometer	Plate–plate	Rotation	Oscillating and transient	15×15×?
Jones and Roberts [24]	(c)	Custom-built Linear oscillator	Plate–plate	Translation	Oscillating	39×39×1
Roberts and Jones [25]	(c)	Custom-built Linear oscillator	Plate–plate	Translation	Oscillating	39×39×3
Goshawk and Jones [28]	(b)	Pull-out apparatus With weights	Plate–plate–plate	Translation	Transient	39×39×1.7
McGuinness and Ó Brádaigh [26]	(d)	Tensile tester	Picture-frame	Translation, pure shear	Transient	200×200×(6.7···9)
Dykes et al. [34]	(f)	Tensile tester	Vee-bending	Translation, bending	Transient	120×40×?
Stanley and Mallon [27]	(e)	Shearing apparatus	Plate–plate–plate	Translation	Transient	(5···10)×10×11

Table 2
Application details of the longitudinal shear characterisation methods presented in table 1. (?) means that information was not explicitly given.

Ref.	Fig. 6	Maximum shear magnitude γ,γ_0	Rates $\dot{\gamma}$ [s^{-1}] ω [rad s^{-1}]	Constitutive model used	Material tested	Number of plies
Groves [17]	(a)	0.01–0.5	0.1–100 [rad s^{-1}]	LVE (Voigt & Maxwell)	CarbonUD/PEEK GlassUD/PP	5–19
Scobbo and Nakajima [21,22]	(b)	0.0150–0.025	64–376 [rad s^{-1}]	LVE (Voigt)	CarbonUD/PEEK CarbonUD/PAS	24 24
Wheeler and Jones [23]	(c)	0.4	0.1–100 [rad s^{-1}]	LVE (Voigt)	CarbonUD/ Golden Syrup	4
Groves et al. [19]	(a)	0.01–0.5	0.1 $\cdots$ 100 [rad s^{-1}]	LVE (Voigt & Maxwell)	CarbonUD/PEEK GlassUD/PP	?
Jones and Roberts [24]	(c)	0.18–0.72	5–100 [rad s^{-1}]	LVE (Voigt)	Nylon/Golden Syrup (model composite)	n/a
Roberts and Jones [25]	(c)	0.06–0.24	0.02–80 [rad s^{-1}]	LVE (Voigt)	Nylon/Golden Syrup (model composite)	n/a
Goshawk and Jones [28]	(b)	0 $\cdots$ 11	0.01–0.7 [s^{-1}]	Newtonian fluid	Nylon/Golden Syrup (model composite)	n/a
McGuinness and Ó Brádaigh [26]	(d)	0–0.2	0.0016–0.1 [s^{-1}]	IFRM + shear thinning	CarbonUD/PEEK	48–64
Dykes et al. [34]	(f)	0–0.8	0.014–0.14 [s^{-1}]	IFRM	Glass/PP	8
Stanley and Mallon [27]	(e)	0–0.5	0.002–0.02 [s^{-1}]	Power law fluid (shear thinning)	CarbonUD/PEEK	80

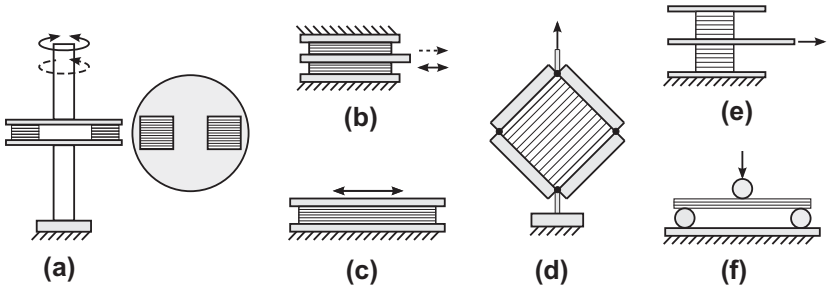

Fig. 6. Illustration of previously developed shear characterisation tests for UD reinforced melts. Tables 1 and 2 refer to the numbering (#).

An alternative set-up was developed by Wheeler and Jones [23]. A specimen is positioned between a fixed upper plate and a lower plate that is connected to an oscillatory drive mechanism, inducing a dynamic translational motion (Fig. 6(c)). The testing material comprised carbon fibres that were embedded within a Newtonian Golden Syrup resin, such that measurements could conveniently be performed at room temperature. The measured dynamic Voigt parameters were reported to be strain magnitude independent. Nevertheless, the sinusoidal load introduction led to responses with distorted sinusoidal shapes but were further independent of strain amplitude. They also reported that a large scatter was observed between identical experiments and the difficulty of producing identical samples with the carbon fibres was also a point of consideration. These reasons gave rise to conduct a research program by Jones and Roberts [24] and Roberts and Jones [25] with a better controllable model composite, utilising the same experimental set-up.

McGuinness and Ó Brádaigh [26] developed a picture-frame experiment to conduct tests with fibre reinforced thermoplastics at high temperatures (Fig. 6(d)). The picture-frame can be mounted in a tensile tester, after which a rhombus-type of shear deformation is induced by the upward displacement of the cross-head. UD carbon PEEK (APC-2) laminates were enclosed by a polymeric diaphragm material. The specimen edges were tightly pressed against the legs of the frame to conduct the shearing deformation properly. Clamping the laminate on both faces would lead to complications, such as fibre tensioning. Such a mechanism is shown in Fig. 7 as an example with a single ply experiment, where it is observed that small fibre misalignments easily result in ply splitting. For cross-plied laminates, shearing deformation was introduced by clamping an over-sized specimen to the faces of the legs via pins. By correcting for the diaphragm foil, longitudinal viscosities were determined as a function of shear rate. By utilising the IFRM model and expressing the viscosities as a function of shear rate, the viscosity could conveniently be described with a power-law relationship.

Stanley and Mallon [27] developed a test set-up (Fig. 6(e)) that shows some similarities with the device that was developed by Goshawk and Jones [28] (Fig. 6(b)). In both cases, specimens are positioned on either side of a centre plate. The other opposite sides of the specimens are pressed against fixed platens. Pulling-out the centre plate introduces a steady transient shear deformation and large strain amplitudes can be obtained. Utilising the IFRM constitutive model just as McGuinness and Ó Brádaigh [26], a power-law relationship was again observed for the tested UD/PEEK (APC-2) material.

The bias extension method is also a well-known test to characterise shear and has successfully been applied to molten thermoplastics with a woven fibre/bundle architecture [29]. This method cannot straightforwardly be applied to UD architectures due to the weak integrity of the laminate at high temperatures. Fig. 7 shows the results of own attempts to characterise UD/PEEK with this method. Specimen deformations were uncontrolled, yielding strain localisation and buckling. The method was, however, successfully applied to thermoset pre-preg materials [30–32] at relatively low temperatures. Integrity is believed to be enhanced by the tackiness of this material.

4. The need for another test

Although the majority of the reviewed methods in the previous section date back from many years ago, no test has been designated yet as the standard test for longitudinal shear

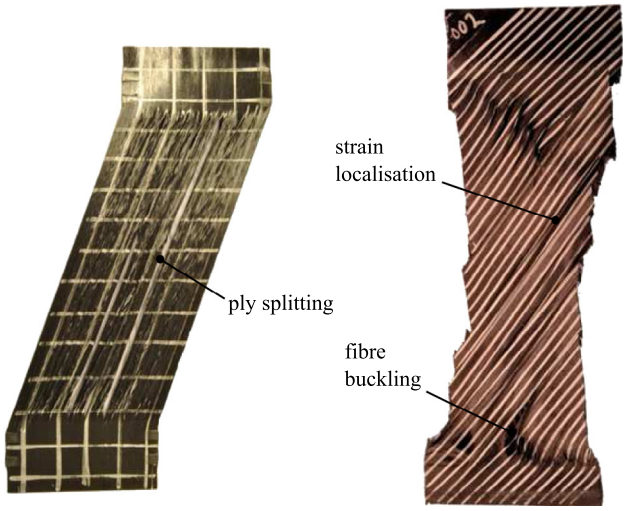

Fig. 7. Own attempts to characterise the shear behaviour of carbon UD/PEEK with the picture-frame and the bias-extension method. (For interpretation of the references to colour in this figure legend, the reader is referred to the web version of this article.)

characterisation of UD reinforced melts. The shortcoming of the tests (a)–(c), and (e) in Fig. 6 is the load introduction being parallel to the fibre directions in the specimen. Resin rich interfaces can be present at the fixture–specimen interfaces and between successively stacked plies [33], which give rise to concentrated shearing deformations at these interfaces. Inter-ply shearing or friction will then be more pronounced, rather than the aimed uniform longitudinal intra-ply shear through the thickness of the specimen. Also the vee-bending set-up used by Dykes et al. [34] in Fig. 6(f) is susceptible to concentrated deformations at the ply–ply interfaces.

Although the picture-frame experiment in Fig. 6(d) is an accepted test for testing fabrics allowing for slight bundle misalignments, misalignments of UD fibres directly result in adverse fibre tensions and specimen defects such as ply splitting (Fig. 7). Moreover, the specimen size required spans a large surface area, which makes temperature uniformity over the entire specimen difficult to achieve. Another drawback is that the majority of the methods discussed utilise custom built set-ups. This hinders the test's accessibility, as the set-up's availability depends on the laboratory's flexibility with respect to the yet unconventional testing requests. Ideally, it should be possible to conduct material characterisation experiments with conventional testing equipment.

The authors believe that the issues addressed above can be circumvented with a novel test to be proposed here, which can be performed with the aid of widely available rheometer devices and standard torsion fixtures. Temperature, temperature uniformity, and atmosphere can be controlled accurately with these devices. The longitudinal shear mechanism is aimed to be characterised with the aid of prismatic bars having a rectangular cross section. Torsional loads will be transferred via the gripping faces indicated in Fig. 3. Load introduction is then perpendicular to the fibre direction instead of the less secured specimen loading parallel to the fibre directions. A detailed analysis of the kinematics is given next, before applying this method in practise,

5. Torsion of bars with a rectangular cross section

The method presented here deals with a prismatic bar that is subjected to torsion. The bar has a constant rectangular cross section, as shown in Fig. 3. Torque M and rotation angle ϕ for linear elastic prismatic bars are related as [35]:

$$M = G_L J \frac{\phi}{L} \quad \varphi = \frac{\phi}{L} \tag{18}$$

in which J is the torsional constant and depends on the cross sectional geometry, L is the free specimen length, and G_L is the elastic shear modulus. The specific rotation angle φ can be used for convenience. It is assumed that the bar consists of UD fibres that run parallel to the rotation axis, although one could account for more complex situations with off-axis fibre alignments [36].

Applying a torsional deformation requires the application of fixtures that introduce these loads. These fixtures restrict the free warping of the cross sections, which results in a stiffening effect [35]. Clamping effects for such rectangular bars were experimentally investigated by Nederveen et al. [37,38]. They developed a torsional pendulum device and a set of fixtures to perform shear property characterisation of homogeneous and isotropic materials. Specimens were clamped and the free specimen length L was varied. The experiments showed deviations in the proportionality between the rotation angle ϕ and the specimen length L, which resulted in a length correction to be used in Eq. (18). A constant length correction was found for sufficiently long bars, as stated by Saint–Venant's principle [39]. Nevertheless, a few remarks were made. Experimental results were compared with theoretical predictions from Timoshenko [35] and Szabó [40], which assumed restricted warping of the cross sections at the end faces of the bar. Deviations between experimental results and model predictions were found. The experimental results were expected to be sensitive to fixture geometry, gripping forces, and material behaviour.

The restriction of warping due to clamping introduces stresses in the axial direction of the bar. These stresses vanish at sufficient distance from the clamping area. It was shown by Timoshenko [35] that the axial stress decays exponentially for isotropic bars for which one bar-end remains plane. Finite element analyses were conducted to investigate such clamping effects for anisotropic bars. The length over which the axial stress decays is dependent on the ratio between the shear and the axial rigidity of the bar. For the high anisotropy considered here (stiff fibres and a more compliant shear property), this length would be very large. For this reason, we assume that the axial stresses are present over the entire specimen length when it is fully clamped at both ends and subjected to torsion. In that case, the torsional constant J for free torsion in Eq. (18) does not hold. Therefore, a lower and an upper bound for the torsional constant will be determined for the case of small rotation angles. For larger rotation angles, the axial fibre stresses contribute rapidly to the torque. This situation is also considered afterwards.

5.1. Lower and upper bounds for the torsional constant

A lower bound for the torsional constant in Eq. (18) is obtained by assuming free warping (free torsion) of the cross section, which reads [35]:

$$J = \frac{1}{3} h^3 w \left(1 - \frac{192}{\pi^5} \frac{h}{w} \sum_{k=1}^{\infty} \frac{1}{(2k-1)^5} \tanh\left(\frac{(2k-1)\pi w}{2h} \right) \right) \tag{19}$$

It assumes transversely isotropic material properties (equal shear properties in the X_1–X_2 and X_1–X_3 planes). The cross sectional dimensions w and h are shown in Fig. 3. The shear strain components read [35]:

$$\gamma_{12}(X_2, X_3) = -\frac{\phi}{L} \frac{8h}{\pi^2} \sum_{k=1}^{\infty} \frac{(-1)^{k+1}}{(2k-1)^2} \left(1 - \frac{\cosh\left(\frac{(2k-1)\pi X_2}{h} \right)}{\cosh\left(\frac{(2k-1)\pi w}{2h} \right)} \right) \sin\left(\frac{(2k-1)\pi X_3}{h} \right)$$

$$\gamma_{13}(X_2, X_3) = \frac{\phi}{L} \frac{8h}{\pi^2} \sum_{k=1}^{\infty} \frac{(-1)^{k+1}}{(2k-1)^2} \left(\frac{\sinh\left(\frac{(2k-1)\pi X_2}{h} \right) \cos\left(\frac{(2k-1)\pi X_3}{h} \right)}{\cosh\left(\frac{(2k-1)\pi w}{2h} \right)} \right) \tag{20}$$

Fig. 8 shows the normalised equivalent shear strain distribution for a narrow and a thicker cross section.

An upper bound of the torsional constant in Eq. (18) is obtained by assuming that each cross section remains plane during loading. The polar moment of inertia for a rectangular cross section can be used for this special case:

$$J_p = \frac{1}{12} wh(w^2 + h^2) \tag{21}$$

Shear strain components then read:

$$\gamma_{12} = -\frac{\phi}{L} X_3 \quad \gamma_{13} = \frac{\phi}{L} X_2 \tag{22}$$

The equivalent shear strain distribution is very different from the free torsion situation, as shown in Fig. 8. The ratio between the polar moment of inertia J_p and the free torsion constant J is shown in Fig. 9. It can be seen that the difference between the lower and upper bound for the torsional rigidity reduces to 20% for square cross sections.

5.2. Small strain dynamic loadings applied to visco-elastic bars

It is aimed to characterise prismatic bars comprising a visco-elastic material. Small strain dynamic testing allows for measuring the storage and loss moduli. The rotation angle and torque can be expressed analogously to Eqs. (11) and (12). By applying the complex notation, we may express these as:

$$\phi^* = \phi_0 \cos(\omega t) + i\phi_0 \sin(\omega t) \tag{23}$$

$$M^* = M_0 \cos(\omega t + \delta) + iM_0 \sin(\omega t + \delta) \tag{24}$$

By replacing the variables in (18) with these complex variants and the introduction of a complex longitudinal shear modulus, one arrives at:

$$M^* = G_L^* J \frac{\phi^*}{L} \tag{25}$$

Since J is a lower bound torsional constant, an upper bound for the separate storage and loss moduli can be determined from dynamic oscillatory experiments:

$$G_L' = \frac{L}{J}\frac{M_0}{\phi_0}\cos(\delta) \quad G_L'' = \frac{L}{J}\frac{M_0}{\phi_0}\sin(\delta) \tag{26}$$

in which the zero subscripts indicate torque and rotation amplitudes, and δ is the phase angle. For square cross sections, lower bounds for these dynamic moduli using J_p will be 16.67% lower than the upper bounds using J, as was concluded from the differences between the torsional constants in Fig. 9.

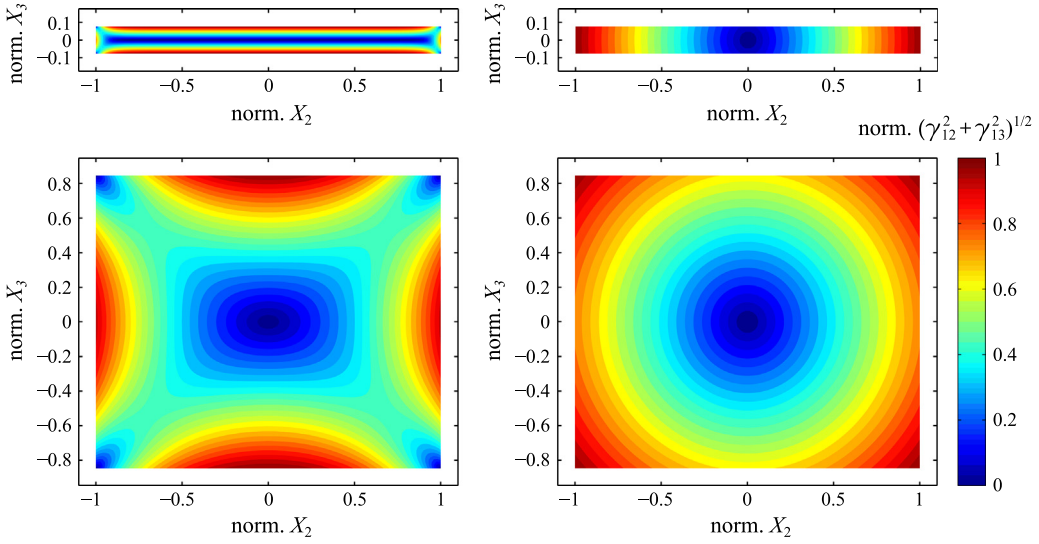

Fig. 8. Normalised equivalent strain distributions within the rectangular cross section. Cross sectional dimensions are normalised as well. Left: assuming warping of the cross section. Right: assuming each cross sectional slice to remain plane (simple torsion). (For interpretation of the references to colour in this figure legend, the reader is referred to the web version of this article.)

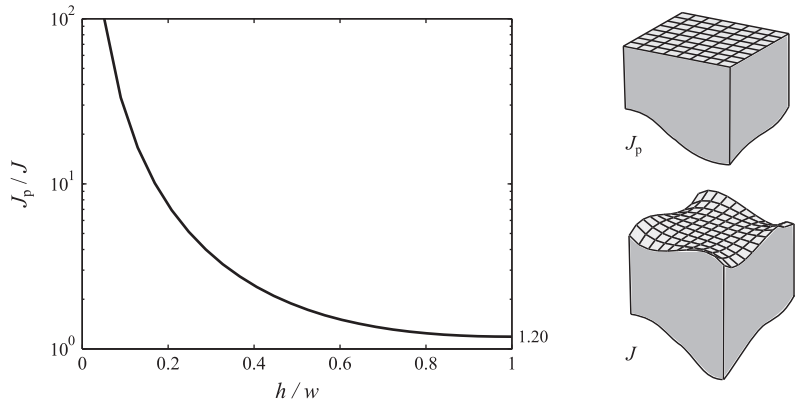

Fig. 9. Left: difference between the torsional constant for the situation where the cross sections are assumed to remain plane (J_p) and the situation where cross sections are free to warp (J). Right: illustration of cross sectional warping for the two extreme cases considered.

5.3. Adverse fibre tensions and larger dynamic deformations

The previous situation of restricted warping is here elaborated by including the effect of fibre tensions, which develop when the end faces of the bar remain at equal distance during torsion. The fibre tensions consequently contribute to the torque, which affects the measured shear property G^*. An analytical model of the fibre reinforced bar with restricted warping is presented, after which the sensitivity of the measured shear property to adverse fibre tensions is investigated.

5.3.1. Kinematics

When the fibre reinforced bar is subjected to torsion and fully clamped at both ends (no warping), each cross sectional slice in the bar rotates rigidly. For this situation, the new coordinates x_i of each point in the rectangular bar are expressed as a function of the initial point coordinates X_i:

$$\begin{aligned} x_1 &= X_1 \\ x_2 &= X_2\cos(\varphi(t)X_1) - X_3\sin(\varphi(t)X_1) \quad \text{with } \varphi(t) = \frac{\phi(t)}{L} \\ x_3 &= X_2\sin(\varphi(t)X_1) + X_3\cos(\varphi(t)X_1) \end{aligned} \tag{27}$$

in which the specific rotation angle φ is a function of time t for dynamic testing. We refer to this situation as simple torsion, since it is analogue to the well-known simple shear situation with an extension to the third dimension. The deformation gradient $\boldsymbol{F}$ maps the old situation X_i to the new situation x_i:

$$\begin{aligned} \boldsymbol{F}(\boldsymbol{X},t) &= \frac{\partial \boldsymbol{x}}{\partial \boldsymbol{X}}|_t \\ &= \begin{bmatrix} 1 & 0 & 0 \\ -\varphi(t)X_2\sin(\varphi(t)X_1) - \varphi(t)X_3\cos(\varphi(t)X_1) & \cos(\varphi(t)X_1) & -\sin(\varphi(t)X_1) \\ \varphi(t)X_2\cos(\varphi(t)X_1) - \varphi(t)X_3\sin(\varphi(t)X_1) & \sin(\varphi(t)X_1) & \cos(\varphi(t)X_1) \end{bmatrix} \end{aligned} \tag{28}$$

The Green–Lagrange strain tensor components then read:

$$\boldsymbol{E} = \frac{1}{2}(\boldsymbol{F}^T\cdot\boldsymbol{F} - \boldsymbol{I}) = \frac{1}{2}\begin{bmatrix} \left(X_2^2\varphi^2(t) + X_3^2\varphi^2(t)\right) & -X_3\varphi(t) & X_2\varphi(t) \\ -X_3\varphi(t) & 0 & 0 \\ X_2\varphi(t) & 0 & 0 \end{bmatrix} \tag{29}$$

The E_{11} term represents the strain in the axial direction, which is related to the square of the specific rotation angle. The E_{12} and E_{13} terms represent the longitudinal shearing, similar to the shear terms in Eq. (22). Transverse shearing does not occur for the assumed kinematics.

The velocity of each point can be determined with (27), which can be used to determine the velocity gradient:

$$\boldsymbol{L} = \frac{\partial \boldsymbol{v}}{\partial \boldsymbol{X}}\cdot\boldsymbol{F}^{-1} = \boldsymbol{D} + \boldsymbol{W} \tag{30}$$

Each second order tensor can be decomposed into a symmetric and a skew-symmetric part, in this case the rate of deformation tensor $\boldsymbol{D}$ and the spin tensor $\boldsymbol{W}$, respectively. The components D_{ij} of the rate of deformation tensor read:

$$\begin{aligned} D_{11} &= D_{22} = D_{33} = D_{23} = D_{32} = 0 \\ D_{12} &= D_{21} = \frac{1}{2}\{-X_3\dot{\varphi}(t)\cos(X_1\varphi(t)) - X_2\dot{\varphi}(t)\sin(X_1\varphi(t))\} \\ D_{13} &= D_{31} = \frac{1}{2}\{X_2\dot{\varphi}(t)\cos(X_1\varphi(t)) - X_3\dot{\varphi}(t)\sin(X_1\varphi(t))\} \end{aligned} \tag{31}$$

where the dots denote the time derivatives of the particular variable.

5.3.2. Constitutive modelling

The torque that would be measured in this situation can be derived from the stress situation in an arbitrary cross section of the rectangular bar. The stresses are determined by the constitutive models considered. A constitutive formulation can be obtained successfully by using a free energy function per unit mass [41]. This function must be an invariant function of the right Cauchy-Green strain tensor $\boldsymbol{C}$ or the Green–Lagrange strain tensor $\boldsymbol{E} = \boldsymbol{E}(\boldsymbol{C})$ in order to deal properly with anisotropy, as was shown by Huétink [42].

The Cauchy stress in case of elastic fibres can be described with the following relation:

$$\boldsymbol{\sigma}_{\mathrm{E}} = \frac{\rho v_{\mathrm{f}} E_{\mathrm{f}}}{\rho_0 l_0^4}\boldsymbol{a}\boldsymbol{a}\boldsymbol{a}_0\boldsymbol{a}_0 : \boldsymbol{E} \tag{32}$$

which was given by Huétink [42] and ten Thije [43]. The densities ρ and ρ_0 cancel out since the assumed kinematics in (27) yield incompressibility and thus $\det\boldsymbol{F} = 1$. A particle within an axially aligned fibre in the bar is initially described with its direction $\boldsymbol{a}_0$ and length l_0. The new direction of the fibre particle is given by vector $\boldsymbol{a}$:

$$\boldsymbol{a} = \boldsymbol{F}\cdot\boldsymbol{a}_0 \tag{33}$$

An impression of the distribution of the new fibre directions for a torsionally loaded bar is shown in Fig. 10. Elastic fibre tensions contribute to the torque with their in-plane decomposed components.

Let the viscous shear behaviour of the assumed fibre reinforced continuum be described with the Newtonian fluid model. The Cauchy stress then reads:

$$\boldsymbol{\sigma}_{\mathrm{V}} = 2\eta_{\mathrm{L}}\boldsymbol{D} \tag{34}$$

where η_{L} is the longitudinal shearing viscosity.

The total stress in each point in the bar can be determined by adding the elastic fibre stresses to the viscous shearing stresses:

$$\boldsymbol{\sigma} = \boldsymbol{\sigma}_{\mathrm{E}} + \boldsymbol{\sigma}_{\mathrm{V}} \tag{35}$$

After substitution of Eq. (28) until (31) into (35), the in-plane components σ_{ij} that contribute to the torque read:

$$\begin{aligned} \sigma_{12} &= \sigma_{21} \\ &= -\frac{1}{2}\{X_3\cos(X_1\varphi(t)) + X_2\sin(X_1\varphi(t))\} \\ &\quad\cdot\left\{v_{\mathrm{f}}E_{\mathrm{f}}\varphi^3(t)\left(X_2^2 + X_3^2\right) + 2\eta_{\mathrm{L}}\dot{\varphi}(t)\right\} \end{aligned} \tag{36}$$

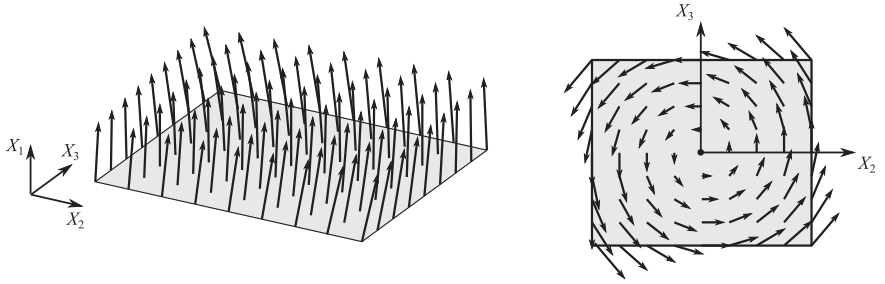

Fig. 10. Impression of the fibre directions $\boldsymbol{a}$ in the new situation at the $X_1 = 0$ plane, for a rotation angle φ. Left: 3D view. Right: top view.

$$\sigma_{13} = \sigma_{31} = \frac{1}{2}\{X_2\cos(X_1\varphi(t)) - X_3\sin(X_1\varphi(t))\} \cdot \left\{ v_f E_f \varphi^3(t)\left(X_2^2 + X_3^2\right) + 2\eta_L\dot{\varphi}(t)\right\} \quad (37)$$

The torque at an arbitrary plane cross section is determined by considering the contribution of the in-plane stresses at each point times their arms, which are measured from the centre of rotation. Adding the contributions of all points yields the following integral formulation:

$$M(\varphi(t)) = \int_{-\frac{h}{2}}^{\frac{h}{2}}\int_{-\frac{w}{2}}^{\frac{w}{2}}\{x_2\sigma_{13} - x_3\sigma_{12}\}\mathrm{d}x_2\,\mathrm{d}x_3 \quad (38)$$

Solving this integral by evaluating the torque at the $X_1 = 0$ plane yields:

$$M(\varphi(t)) = M_E + M_V = \varphi^3(t)\frac{v_f E_f}{160}\left(w^5 h + h^5 w + \frac{10}{9}w^3h^3\right) + \dot{\varphi}(t)\frac{\eta_L}{12} \cdot (w^3h + wh^3) \quad (39)$$

where the total torque is divided into an elastic and a viscous part.

5.3.3. Sensitivity analysis

The effect of fibre tensions on the measured response was investigated for the case that one assumes the free torsion situation, whereas the specimen is actually clamped in such a way that warping is restricted. The aspect ratio of the cross section, material parameters, rotation amplitude and rotation frequency were varied. The analysis procedure is schematically shown in Fig. 11.

It is convenient to introduce a dimensionless number that represents the combination of the material parameters used:

$$\mathrm{Fd} = \frac{v_f E_f}{\omega\eta_L} \quad (40)$$

This number is referred to as the fibre dominance number. The term ω is the already introduced angular frequency. As an example, a fibre dominance number of 1.33×10^6 represents the situation of a bar with longitudinal shear viscosity $\eta_L = 1000$ Pa s, fibre volume fraction $v_f = 0.6$, and fibre elasticity modulus $E_f = 221$ GPa, which is tested at $\omega = 10$ rad/s.

In case of dynamic testing, the rectangular bar is subjected to an oscillating rotation angle with amplitude φ_0:

$$\varphi(t) = \varphi_0\sin(\omega t) \quad \dot{\varphi}(t) = \varphi_0\omega\cos(\omega t) \quad (41)$$

The torque was evaluated by substituting Eq. (41) into (39) for a given Fd number. The torque amplitude M_0 and the phase angle δ were subsequently determined by means of spectral analyses. This was achieved by applying a Fast Fourier Transform (FFT) and a Cross Power Spectral Density (CPSD) algorithm, which are available in MATLAB.

5.3.4. Results

Without the presence of adverse fibre tensioning effects, one would ideally measure the desired material shearing parameter G_L^*. It would only have an imaginary part $G_L'' = \eta_L'$, since a purely Newtonian shearing viscosity η_L was assumed in (34). The deviation between the actual viscosity η_L and the measured dynamic viscosity is expressed as:

$$\frac{|\eta^*|}{\eta_L} \quad (42)$$

which equals to unity when no fibre tensioning is present. The results of the sensitivity study are presented for a narrow and a square cross sectional geometry in Fig. 12. Whereas the results can be represented as a function of cross sectional aspect ratio, the rotation angle amplitude φ_0 necessary to achieve a certain strain amplitude γ_0 is dependent on the actual cross sectional dimensions (see Eqs. (20) and (22)). Realistic dimensions ($h = 1\cdots10$, $w = 10$ mm) were used to generate the rotation angle axis on top of the figures. This rotation angle was further determined from the maximum strain amplitude γ_0 that appears in the case of free torsion (no clamping effects), which is shown by the second x-axis. The evaluated model assumes no warping, which results in a different maximum strain γ_0 as shown by the third x-axis in grey.

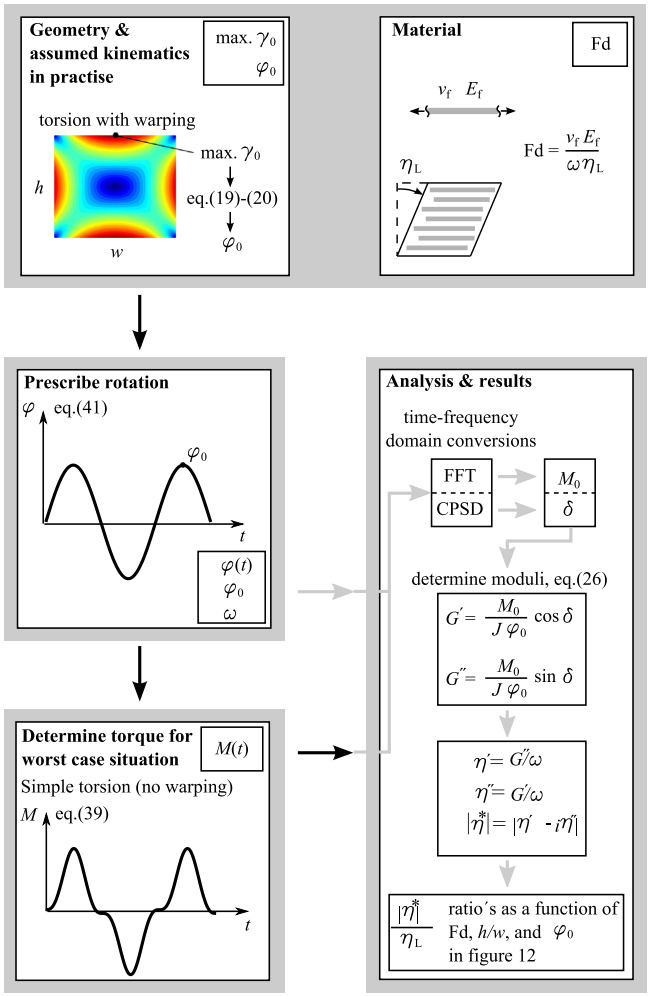

Fig. 11. Flow chart of the analysis procedure. (For interpretation of the references to colour in this figure legend, the reader is referred to the web version of this article.)

Fig. 12(a) shows the deviations for the narrow cross section as a function of strain amplitude and fibre dominance number. The measured material property is increasingly overestimated for increasing rotation angles. As expected, a larger fibre dominance number results in larger overestimations of the shearing property. For the rotation angle φ_0 considered, the maximum shear strain γ_0 for free torsion and for restricted warping deviate highly as well. This implies that the actual shear strain amplitude that appears in practise is quite uncertain, as the actual clamping effects in practise are unknown.

Fig. 12(b) shows the deviations for the square cross section. Also here, an increasing rotation angle and fibre dominance number result in an increasing overestimation of the measured shear

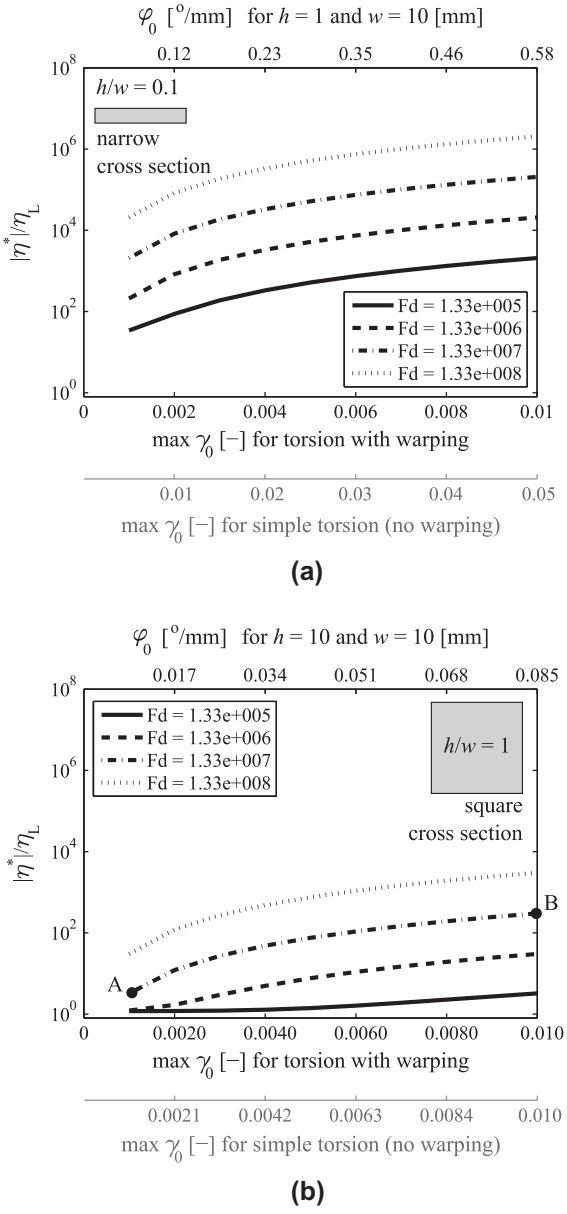

Fig. 12. Deviations of the measured complex viscosity $|\eta^*|$ with respect to the actual shearing viscosity η_L when fibres are tensioned according to the simple torsion model. (a) Narrow cross section. (b) Square cross section.

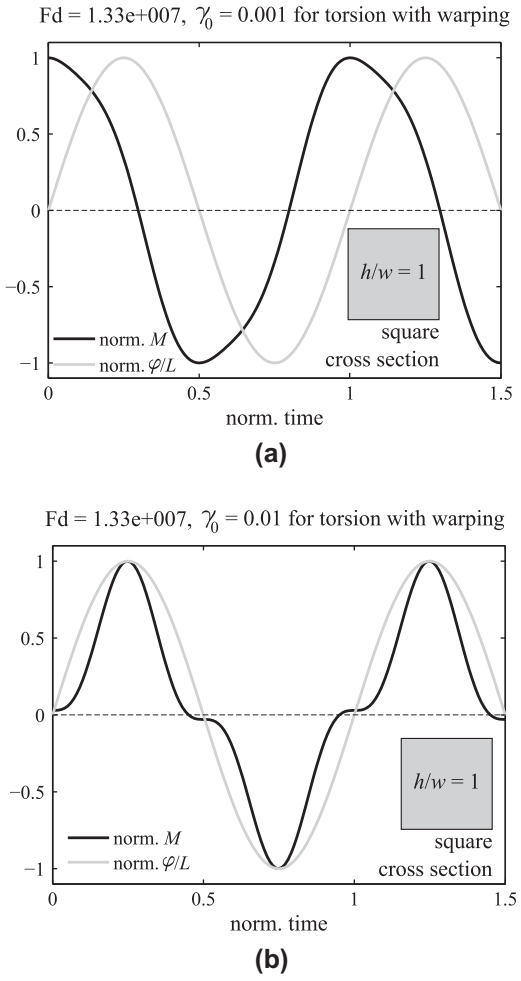

Fig. 13. Torsional responses as invoked by a sinusoidally applied rotation. (a) Parameter input as represented by point A in Fig. 12(b). (b) Parameter input as represented by point B in Fig. 12(b).

property. The overestimations are smaller than those for the narrow cross section, for a certain fibre dominance number. Compared to the narrow cross section, smaller rotation angles are necessary to achieve a certain strain amplitude. In the contrary to the narrow cross section results, the difference between the shear strain amplitudes for the free torsion and the restricted warping situation is negligible (lower two x-axes). In order to get an impression of the distorted responses, Fig. 13 shows the model predictions for points A and B indicated in Fig. 12(b). Clearly, the elastic fibres distort the purely sinusoidal torsional response (Fig. 5), as assumed by the LVE theory. These responses were validated with the aid of finite element analyses [44].

5.4. Torsion bar guidelines

Guidelines have been established for the torsion bar geometry. These are based on the previous kinematic analyses and the practical experience of the authors. Close to square cross sections of $h/w = 0.85$–1 are advised, because:

- Distorted torsional responses and therefore the deviation between the measured and actual shear property are then minimised.
- The difference between the maximum strain amplitude for free torsion and bars with restricted warping is minimal for square cross sections.
- The thicker the specimen, the better is the integrity of the specimen at high temperatures in practise.

Apart from the cross sectional aspect ratio, the specimen width and thickness can be determined according to the available space in the rheometer device and fixtures and the load range of the instrument. A larger torque is required for larger cross sectional dimensions. These can be determined such that the envisioned torque amplitude is within the accurate measurement range of the load cell. Large specimen lengths are advised. A larger length results in a larger volume to shear, which results in a better averaged response of the specimen. However, clamping effects are not weakened for larger lengths due to the high anisotropy. Moreover, the length is limited by the available space in the testing device and the acceptable temperature deviation within the specimen.

6. Experimental work

An experimental program was carried out to investigate the specimen responses obtained with this method. Firstly, a description of the used equipment, specimens, and testing procedure is given. Conditions that lead to linear and non-linear behaviour are explored. Subsequently, the linear responses are elaborated in more detail.

6.1. Equipment

A standard Anton Paar® MCR501 rheometer was used, as shown in Fig. 14. It is able to perform rheological tests by conducting steady and oscillatory rotations. Torsional loads are generated by a synchronous electrical motor and can either be rotation or torque controlled. The rotation controlled mode was used as it yields the most stable responses for the type of experiments considered here.

The modular design allows for the use of different fixture types. For this study, the standard SRF-12 solid torsion bar fixtures were selected, which are generally used to perform measurements on solid bars in torsion. Storage and loss moduli are conventionally measured as a function of temperature, for example to determine glass transition temperatures of plastics [45]. Rectangular bar specimens with thicknesses up to 12 mm can be gripped at the end faces of the specimen, as shown in Fig. 14. One gripping face is part of a rigid modular block, whereas the opposite gripping face consists of a moveable plate and is loosely guided by two little pins. In order to achieve stable gripping for soft materials, the standard fixture was modified. The gripping is now introduced by two bolts instead of one.

6.2. Specimen geometry and production

The selection of specimen dimensions is based on the guidelines presented in Section 5.4. Specimens were produced with the CETEX® TC1200 PEEK/AS4 pre-preg material from Ten Cate. The pre-preg material consists of a uni-directional AS4 carbon fibre reinforcement and a PEEK thermoplastic matrix (UD/PEEK). Glass transition and melt temperature of the PEEK polymer [46] are 143 °C and 343 °C, respectively. One pre-preg ply measures a thickness of 0.14 mm. Thick UD laminates were manufactured by stacking 80 equally oriented plies of the pre-preg material. The stack was positioned in a framed mould, which was utilised in order to minimise transverse flow. The framed mould was transferred to a flat platen press for consolidation. The temperature and pressure cycle were applied according to the material's datasheet. The resulting laminate measured a thickness of 11 mm and a nominal fibre volume fraction of 59.3%. Specimens were subsequently cut from the laminate with a diamond wheel saw to yield dimensions of $w = 13$, $h = 11$, and $\widetilde{L} = 60$ mm, as indicated in Fig. 15. The specimens were dried in a vacuum oven at 80 °C prior to testing.

Instead of the advised square cross sectional geometry, the selection of dimensions 13×11 mm was driven by practical reasons. The specimen thickness of 11 mm can be obtained by consolidating a stack of 80 pre-preg plies, however, larger stacks become impractical to handle. A width of 13 mm was employed, because it was a convenient dimension to control the alignment of the specimen during its positioning in the rheometer.

6.3. Testing procedure

The specimen is carefully positioned in the fixtures, such that it is well aligned with the rotation axis. The specimen ends are gripped between the modular blocks and the guided plates, as shown in Fig. 14. The bottom surface of the specimen rests on the surface of the lower static fixture. A gap of 0.5–1.0 mm between the top surface of the specimen and the top fixture is ensured to allow for specimen movement in the axial direction of the bar, which is driven by thermal expansion when heated. Herewith, the development of adverse compressive forces is prevented.

A low flow of nitrogen gas is applied within the heating chamber in order to avoid polymer degradation effects that are driven by the presence of oxygen [47]. The testing temperature is controlled with a thermocouple. Tests with a specimen equipped with 3 embedded thermocouples indicated that a steady state temperature distribution in the specimen was achieved in approximately 10–15 min. Once the cavity temperature reaches the set temperature, these levelling times are ensured prior to testing. The temperature in the specimen deviates less than 10 °C from this set temperature.

Torsional responses are measured by applying oscillating rotations to the upper fixture. Storage and loss shear moduli are determined with Eq. (26). Only these upper bound moduli are shown next for a clear presentation of the results, however, it must be kept in mind that the lower bound moduli could be ≈16% lower.

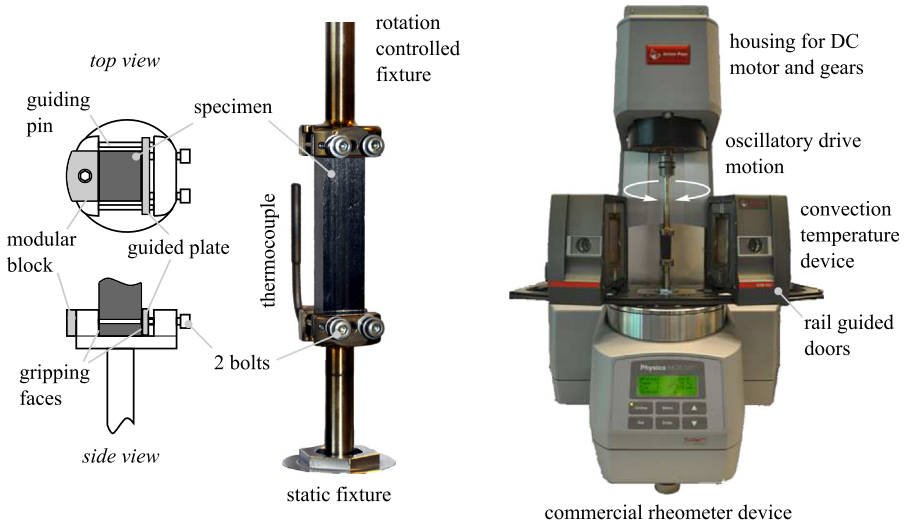

Fig. 14. Left: actual torsion specimen and fixtures. Right: commercially available rheometer. (For interpretation of the references to colour in this figure legend, the reader is referred to the web version of this article.)

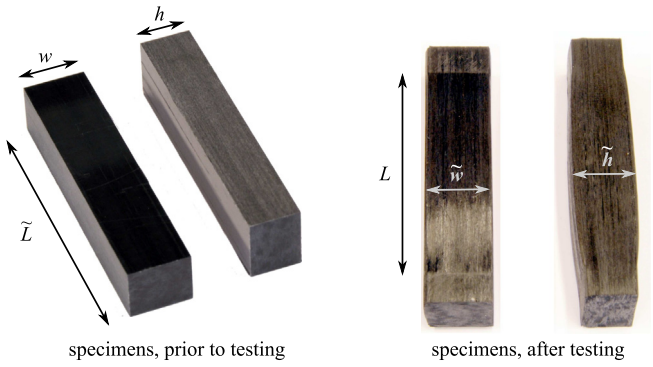

Fig. 15. Left: UD/PEEK specimens as cut from the laminate. Right: specimens after re-heating to processing/testing temperature. Frozen in consolidation stresses are released resulting in deconsolidation, which distorts the ideal testing geometry. (For interpretation of the references to colour in this figure legend, the reader is referred to the web version of this article.)

The maximum shear strain that appears in the rectangular cross section is used as a reference throughout all the analyses. By assuming free torsion, Eq. (20) shows a maximum shear strain at the centre of the longest edge of the cross section.

6.4. Explorative measurements and non-linear behaviour

Separate frequency sweeps with different strain amplitudes γ_0 were applied to explore the linear and non-linear behaviour of the material. Fig. 16 shows the dynamic moduli to be dependent on the strain amplitude, indicating non-linear material behaviour. The moduli are large for the small strain amplitude, but rapidly decrease when the larger strain amplitude γ_0 is applied.

6.4.1. Amplitude dependency

Rapidly decreasing storage and loss moduli for increasing strain amplitudes were also observed by Groves et al. [19] and Scobbo and Nakajima [22] for a similar composite system. It is interested to note that Jones and Roberts [24] also reported this drop as measured with a custom-built linear oscillator. However, they tested a model composite comprising a Golden Syrup with embedded nylon fibres instead of a UD/PEEK system. By increasing the fibre volume fraction, they observed an increasing drop in the moduli for increasing strain amplitudes. An explanation can be given by

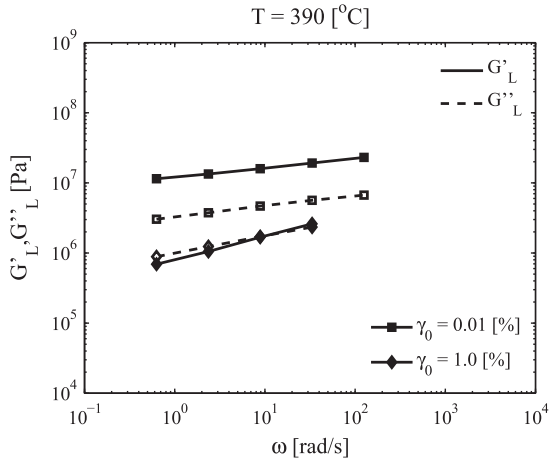

Fig. 16. Frequency sweeps with different strain amplitudes applied to UD/PEEK specimens. Upper bounds for apparent longitudinal shear moduli G'_L and G''_L are shown only.

considering the work of Nguyen and Boger [48]. Instead of fibre reinforced melts, they reported on media with suspended particles such as carbon black in a Newtonian liquid. Such media show a critical strain amplitude between 0.01% and 5% in general. It was reported that the dynamic moduli decrease rapidly beyond this critical strain amplitude as also observed by Jones and Roberts, and in Fig. 16. The intrinsically different rheological behaviour of suspended media compared to the same unfilled (neat) media can be explained by the presence of particle–particle and particle–polymer interactions, respectively caused by, for example, the presence of friction [49] and physical bonds [50]. Analogously, the measured behaviour here may be attributed to fibre–fibre and fibre–polymer interactions. This is further supported by the results of Jones and Roberts, as the change of the dynamic moduli for increasing fibre volume fractions [24,25] is comparable to that observed in suspended media for an increasing particle volume fraction [48].

6.4.2. Waveforms

According to the LVE theory, the material behaves linearly when a sinusoidally applied deformation (rotation angle) results in a purely sinusoidal stress (torque M) response. Non-linear material behaviour is indicated by deviations from the primary sine wave. Fig. 17 shows the waveform data for several measurement points in Fig. 16. Pure sine wave responses are observed for the small strain amplitude of 0.01% at all frequencies. Sine wave distortions can be observed at the larger shear amplitude of 1.0%. Such distortions are defined in the field of large amplitude oscillatory shear (LAOS) testing [51]. The observed shapes are referred to as backward tilted shoulder waves. As shown for the data with $\gamma_0 = 1.0\%$, increasing the frequency decreases the backward tilted distortion.

Groves et al. [19] also performed high temperature shear tests on a carbon UD/PEEK composite by means of an oscillatory plate–plate set-up. It was reported that deviations from the primary sine wave were observed for low frequencies and small strains, and at high frequencies and large strains. Another publication of Roberts and Jones [25] showed the waveform data obtained from experiments with the earlier mentioned model composite (nylon fibres embedded in Golden Syrup, tested with their custom-built linear oscillator) with a fibre volume fraction of 60%. Pure sine waves were found for relatively large shear strains of 6% at frequencies between 1 and 80 rad/s. Larger strain amplitudes resulted in backward tilted shoulder waves, as was observed here as well. The distortion was also smaller for higher frequencies. Flat topped sine waves were shown at frequencies lower than 0.1 rad/s, which was explained to be caused by yielding of the material [48].

6.5. Small strain measurements in the linear regime

Strain and frequency sweeps were conducted at 390 °C for five UD/PEEK specimens. To assess the repeatability of the experiment, two subsequent runs with identical sweep settings were performed. For the small strain experiments to be discussed next, all subsequent runs reproduced well.

Fig. 18 shows the averaged moduli determined by the amplitude and frequency sweeps for the five specimens. Standard deviations read between 20% and 30%. The solid lines represent the storage moduli, whereas the dashed lines represent the loss moduli. Prior to the actual forming process in general, pre-consolidated fibre reinforced thermoplastic laminates show deconsolidation in the thickness direction when heated above the melting point. The torsion bar specimens show these effects as well. This is not an issue as it is aimed to characterise the shear properties in the material's configuration as present in forming conditions. Nevertheless, Fig. 15 shows that the specimens will expand non-uniformly due to the presence of the fixtures. This leads to a

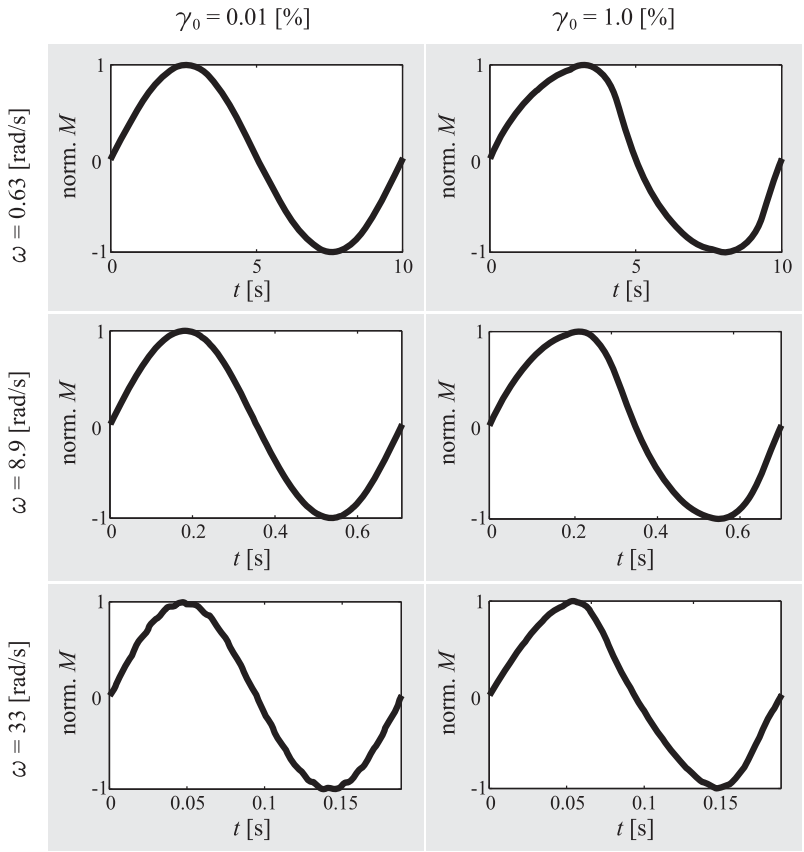

Fig. 17. Waveforms as a function of strain amplitude and angular frequency for the UD/PEEK specimens.

non-uniform torsional rigidity. The dynamic moduli in Eq. (26) were for this reason calculated for two geometries. The black lines show the results by assuming the initial geometry as shown in the left of Fig. 15. The grey lines were obtained by assuming a uniform cross section over the specimen's length as well, but now using the maximum width and thickness as they appear in the expanded specimen after testing.

Amplitude sweeps were conducted within a strain range that covered approximately one decade only with a maximum strain amplitude of ≈0.1%. Fig. 18 shows the results for the sweeps at a fixed frequency of 6.28 rad/s. The measured shear moduli were constant for the investigated shear strain range, which implies linear material behaviour. As concluded from the exploratory measurements in the previous section, larger strain amplitudes result in non-linear material behaviour. It is possible that a permanent change of the specimen's structure, such as fibre migration, develops beyond this point. This could lead to a different specimen response. Larger strain amplitudes were therefor not applied.

Frequency sweeps were applied subsequently with shear strain amplitudes of $\gamma_0 = 0.1\%$. The measured dynamic moduli are shown in Fig. 18. The dynamic and complex viscosities are shown in Fig. 19. Approximately four decades of angular frequency were covered, varying between 0.126 and 503 rad/s (0.02–80 Hz). Good reproducibility was obtained for all measurements, as indicated by the standard deviations for the sample of five specimens.

Test at different temperatures above T_m were carried out as well, for which the results are shown in Fig. 20. Clearly, the temperature does not influence the moduli within the small strain regime.

6.5.1. Alternative load introduction

Although realistic responses were found so far for the composite system, experiments with an alternative clamping method were conducted for completeness. As shown in Fig. 21, two aluminium plates of 13 × 12 × 2 mm were attached to both ends of the specimen. These were initially attached by using an adhesive to support proper positioning of the plate. The adhesive disintegrated when the specimen was heated to the testing temperature. A grid of 3 × 4 holes was drilled through the plate and 3 mm through the specimen itself to resolve this problem. Little pins were cut from a weld wire with a diameter of 1 mm. These were pressed into the drilled holes such that a rigid connection between the pins and the aluminium plate was established. Torsional loading is now solely introduced via these pins. The assembly was positioned in the rheometer, where the fixtures grip at the aluminium plates. In this way, the specimen side planes were not in contact with the standard fixtures. When heated above the melting temperature, uniform deconsolidation of the specimen occurred due to the absence of grips on the side planes.

Frequency sweeps were conducted at 390 °C. The measured dynamic moduli are shown in Fig. 22. Similar material behaviour was found, as compared to the averaged responses that were found for the tests with the preferred simple gripping mechanism in Fig. 14.

7. Discussion

7.1. Comparison with neat polymer characteristics

Fig. 18(b) showed the measured moduli of the composite system to be weakly dependent on frequency. A constantly increasing slope of moduli versus frequency can be observed for the range of frequencies considered. The storage terms are consistently larger than the loss terms within the range of investigated parameters. This behaviour is substantially different from the polymer characteristics without the presence of fibres.

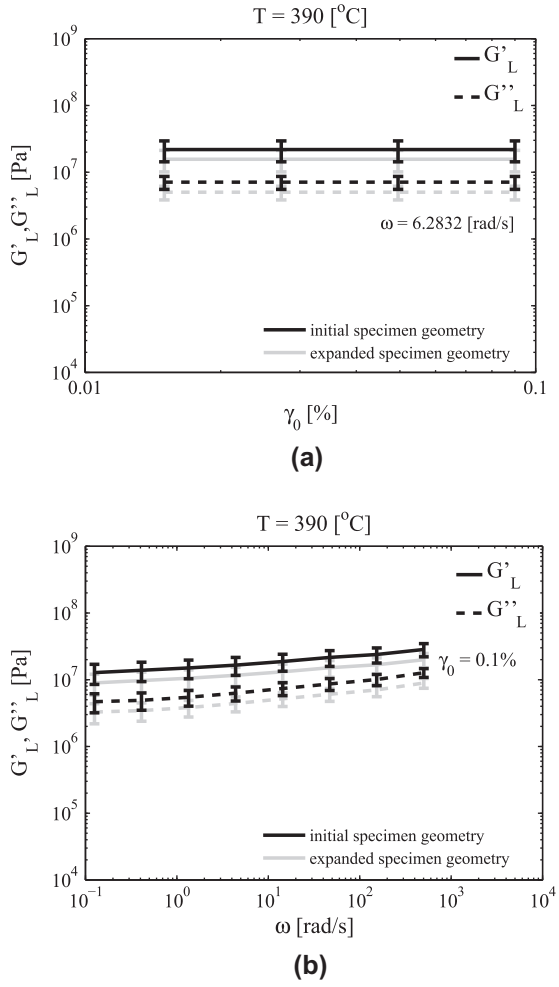

Fig. 18. Averaged apparent dynamic moduli for the UD/PEEK material as a function of strain amplitude γ_0 (a) and angular frequency ω (b).

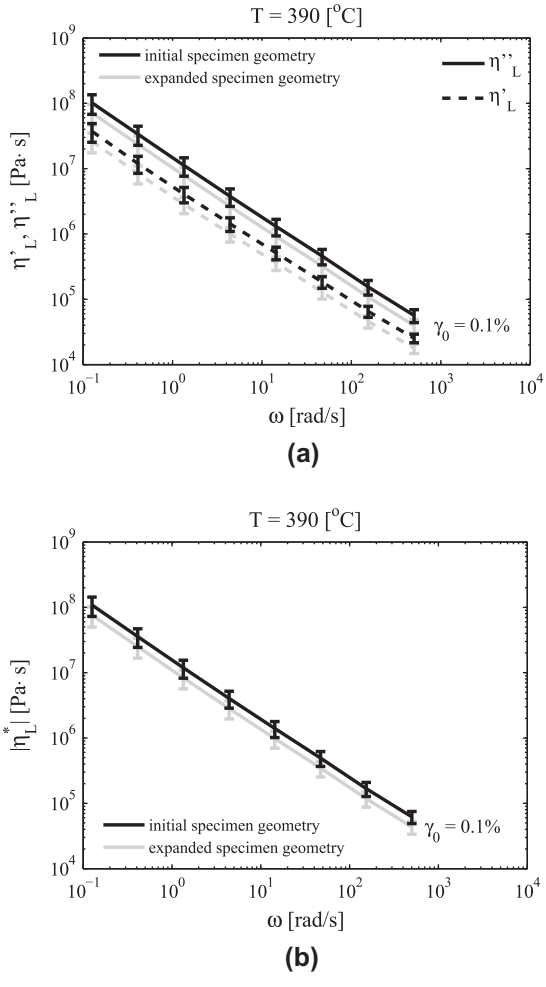

Fig. 19. Averaged apparent dynamic (a) and absolute complex (b) viscosities for the UD/PEEK material, as a function of angular frequency ω.

Fig. 23(a) shows the typical dynamic moduli of the neat PEEK polymer, which were obtained with a rotating plate–plate set-up. Frequency sweeps were conducted with a strain amplitude of $\gamma_0 = 1.0\%$ at which linear responses were obtained. A larger frequency dependency of the moduli is observed when compared to the responses of the composite system in Fig. 18(b). Moreover, a dominating loss modulus is present, which is representative for many molten polymers. The dynamic viscosities are constant at low frequencies. A steady shear measurement result has been added to Fig. 23(b) showing the steady shear viscosity. The dynamic and steady shear relations show similar trends. This observation is common for neat polymers in their molten configuration, which resulted in the empirical translation given by the Cox–Merz rule [52]. It relates the dynamic absolute complex viscosity and the transient steady shear viscosity as:

$$\eta(\dot{\gamma} = \omega) \simeq |\eta^*(\omega)| \tag{43}$$

Nevertheless, this relationship does not hold for suspended media in general, such as the composite system considered here.

Focusing on the linear material behaviour of the composite melt, the elastic dominance is most likely caused by the presence of the fibres. For the sake of argument, imagine a system containing fibres that are well aligned and uniformly distributed such that no fibre–fibre contacts are present. Then one should measure responses that are similar to the neat polymer characteristics. Next to the global or apparent shear rate, small spaces between the rigid

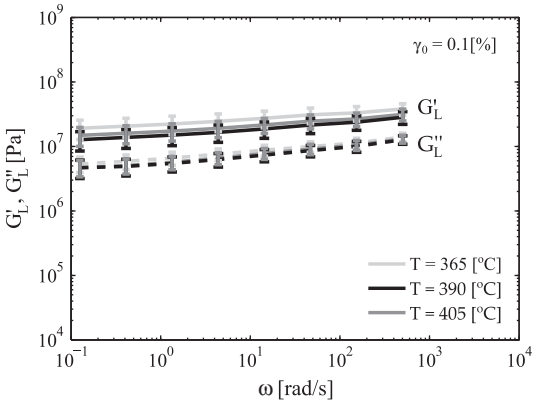

Fig. 20. Apparent dynamic moduli for the UD/PEEK material at three temperatures.

fibres lead to higher shear rates locally. This ideal situation was considered by Pipes et al. [8], where solely the fibre volume fraction and the packing geometry determine this shear rate magnification. Consequently, the neat polymer viscosity characteristic in Fig. 23 shifts horizontally towards smaller shear rates. The considered ideal alignment is unrealistic for the fibre volume fractions considered here, which is approximately 60%. As supported by the micrograph in Fig. 4, multiple fibre interactions are present.

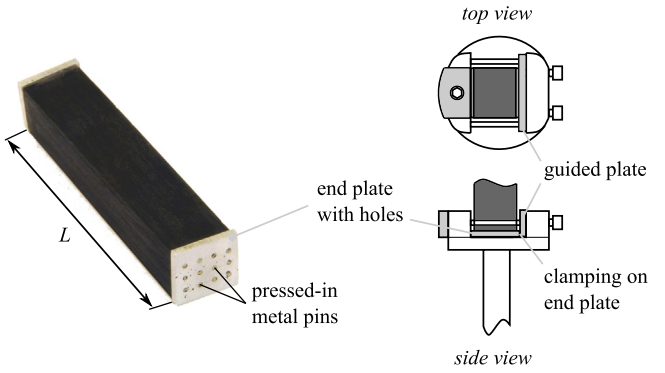

Fig. 21. Alternative fixture with short metal pins to conduct the torsional loads. The standard SRF-12 fixtures are used to clamp the aluminium end plates. (For interpretation of the references to colour in this figure legend, the reader is referred to the web version of this article.)

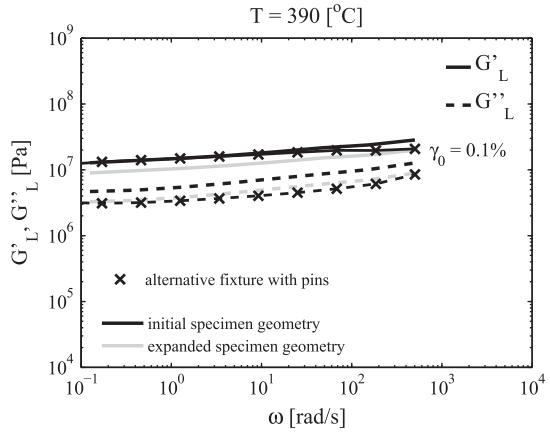

Fig. 22. Frequency sweeps and their resulting apparent dynamic moduli for the UD/PEEK material. A comparison between the preferred simple gripping with existing fixtures (solid and dotted lines from Fig. 18(b) without error bars) and the alternative fixture with pins (crosses).

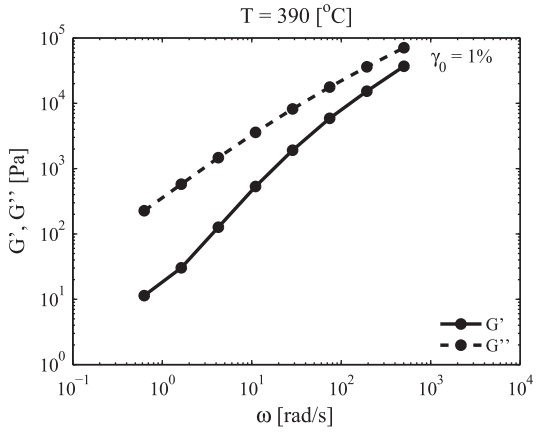

(a) Dynamic moduli.

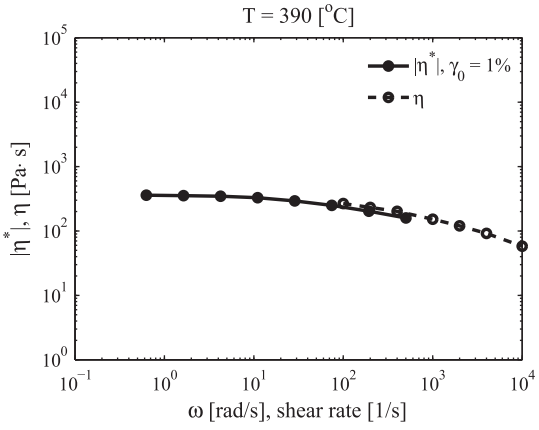

(b) Absolute complex viscosity and transient steady shear viscosity.

Fig. 23. Frequency response of the neat PEEK polymer at 390 °C and $\gamma_0 = 1\%$, obtained with a parallel plate set-up.

These invoke the measured elastic effects during deformation. This also explains the temperature independent moduli (Fig. 20), as temperature influences the polymer melt only and not the fibrous structure itself. Similar assumptions have been argued and considered by Gutowski [1] in order to model the elastic response during laminate consolidation cycles. The elastic behaviour was also observed in the results of Stanley and Mallon [27], who measured the longitudinal response of APC2-PEEK with a translating plate–plate set-up.

7.2. The nearly frequency independent moduli

The plateau-like characteristics of the dynamic moduli in Fig. 18(b) have also been observed by Roberts and Jones [25] for Golden Syrup with nylon fibres. Manual deposition of the nylon fibres allowed for a controlled fibre volume fraction. Increasing the fibre volume fraction from 0.1 to 0.7 resulted in a plateau developing for both the storage and loss moduli at lower frequencies. As discussed by Nguyen and Boger [48], more particle–particle and particle–polymer interactions develop for an increasing particle volume fraction. As argued by Onogi et al. [53], this leads to a formation of a network structure such that much longer relaxation times develop, compared to the longest relaxation time of the neat polymer. The relaxation time can be seen as the time needed by the material to adjust to the applied stress or deformation, which is ≈0.05 s for PEEK [54]. The relaxation time of the composite is relatively large compared to the lowest testing frequency considered (high Deborah number [55]), and therefore a solid-like response is observed. Moreover, the low frequency plateaus in the dynamic moduli suggest the presence of yield stress behaviour in large strain steady shear tests [48]. A yield stress value was indeed found in the analysis of Groves [17] for the plate–plate shear characterisation test. It must be noted, however, that this was implicitly determined with the dynamic data and the use of dynamic Maxwell parameters [20], instead of the conventionally used dynamic Kelvin–Voigt moduli.

In the more general sense, the behaviour observed is a characteristic of a visco-elastic solid or weak gel [56]. Similar dynamic responses have been observed in other fields of research. Examples of media that show the same weak frequency dependency are biomass slurry [57], chestnut flour doughs [58], peanut butter [56], and brains [59].

7.3. Other characterisation results for UD/PEEK

The obtained characteristics are compared in Fig. 24 with frequency data from other characterisation tests applied to the UD/PEEK material. However, these reference data were obtained twenty years ago approximately. This comparison must therefore be interpreted with care, since polymer blends and fibre architectures are usually modified over the years. Groves et al. [19] utilised

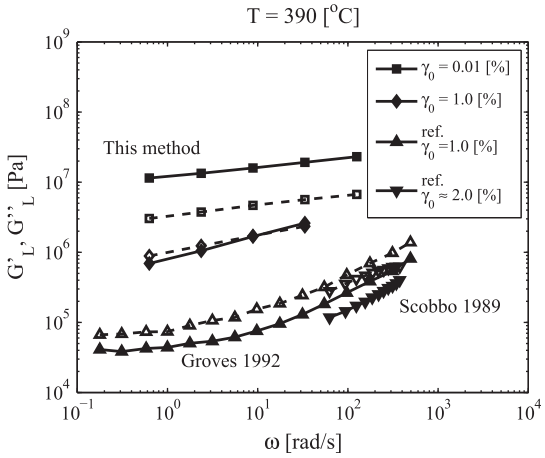

Fig. 24. Comparison of apparent dynamic moduli at 390 °C, with respect to those obtained from other shear characterisation techniques. Groves et al. [19] utilised a rotating plate–plate set-up. Scobbo and Nakajima [21] utilised a translating plate–plate set-up.

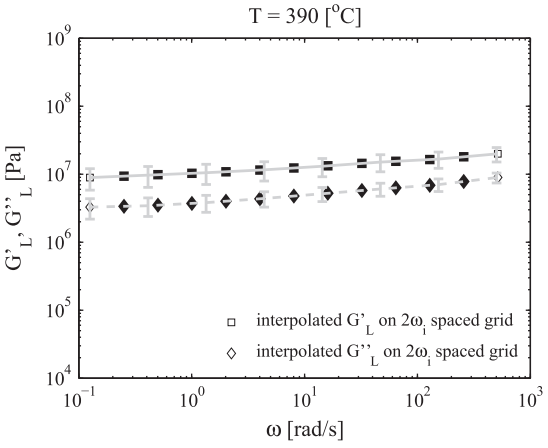

Fig. 25. Averaged frequency sweep data for the expanded UD/PEEK specimens. The experimental data is interpolated to a grid, as indicated with the square and rhombus type markers.

the previously mentioned rotating plate–plate set-up, and Scobbo and Nakajima [21] used a translating plate–plate configuration. They used shear strain amplitudes of 1.0% and 2.0%, respectively. The moduli show much lower values, but it was shown by Groves et al. [19] that the material behaves non-linearly for relatively small strain amplitudes. This agrees with our observations that the dynamic moduli decrease rapidly beyond the transition from linear to non-linear strain responses. Such effects may partially explain the differences in this figure.

Next to a dominating loss modulus, both Groves et al. and, Scobbo and Nakajima found a larger frequency dependency of the moduli. As argued by Stanley and Mallon [27], the formation of resin rich layers influences the load introduction into the reinforced part of the melt. As a result, inter-ply slip is likely to dominate the specimen deformation, instead of the intended intra-ply shearing itself. They confirmed such behaviour with their own measurements, where the specimens were loaded parallel and perpendicular to the inter-ply interfaces. Both the methods of Groves et al. and, Scobbo and Nakajima only introduce shear forces parallel to the inter-ply interfaces and thus parallel to the fibre direction. This is substantially different from the load introduction here. Torsional loads are introduced perpendicular to the fibre direction, which might also explain the differences observed.

As a final note to all shear characterisation methods, it is questionable whether the assumption of transverse isotropy (equal longitudinal shear moduli in the 12 and 13 planes) holds (see Fig. 3). In combination with the type of load introduction, parallel or perpendicular to the fibres, a difference between these moduli possibly affects the ratio between γ_{12} and γ_{13} at a certain point in the specimen, thereby deviating from the theoretical shear strain distributions that were assumed in Eq. (20).

The introduced torsion bar method was shown to yield plausible shear characterisation data. The small strain behaviour is important to describe the intra-ply shear mechanisms in laminate forming prediction software. The method shows good potential to become a standard test in the future, considering the relatively small effort to perform the experiments and the repeatability of the data obtained.

8. Conversion of the linear responses to the transient domain

The shear behaviour for small strains is now known in the frequency domain. Since the forming process of hot laminates takes

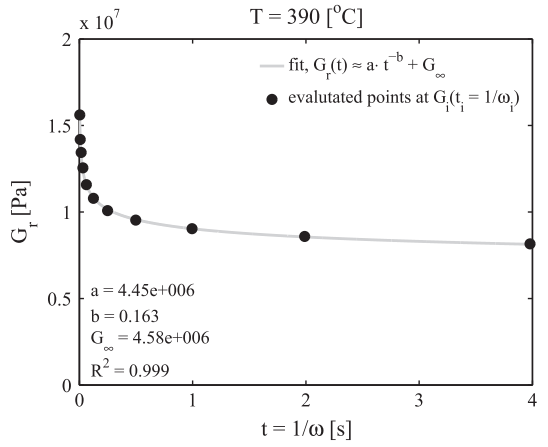

Fig. 26. Relaxation function G_r evaluated at several points $t_i = 1/\omega_i$ according to the finite difference scheme in (46).

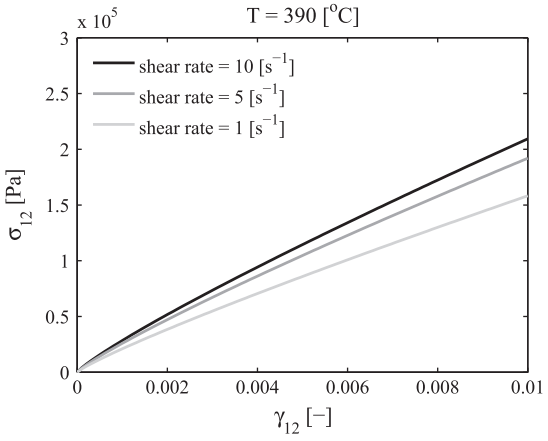

Fig. 27. Shear stress–strain response according to Eq. (47) for several constant shear rates.

place in the transient time domain, the measured characteristics (Fig. 18(b)) have to be translated. The earlier mentioned empirical Cox–Merz rule [52] in Eq. (43) is often used for neat polymer melts with a dominating loss modulus, as well as showing shear thinning behaviour at larger shear rates. Generally, this rule cannot be

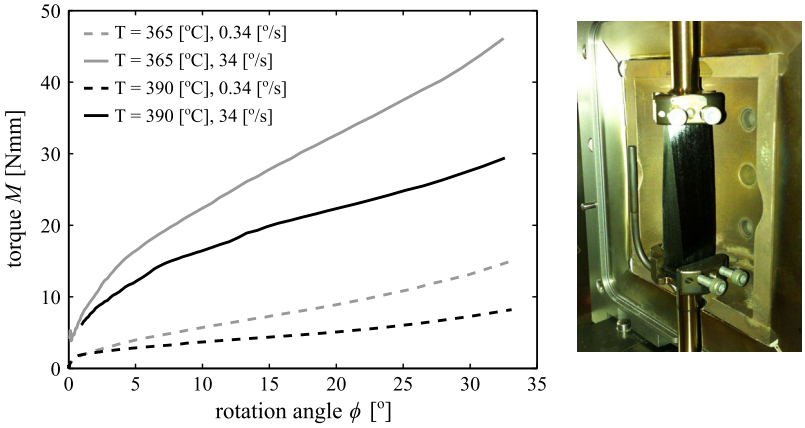

Fig. 28. Explorative large shear characterisation results: torsional responses as a function of rotation angle are shown for instantaneously applied constant rotation speeds. (For interpretation of the references to colour in this figure legend, the reader is referred to the web version of this article.)

applied for media with suspended particles that interact during deformations. This was for example shown by Kitano et al. [60] for short glass fibre filled polyethylene.

Transient deformations of linear visco-elastic materials are described via the following constitutive relationship [7]:

$$\sigma_{12}(t) = \int_{s=-\infty}^{t} G_r(t-s)\dot{\gamma}_{12}(s)\mathrm{d}s \tag{44}$$

also known as the Boltzmann integral. Here, σ_{12} is the shear stress, $\dot{\gamma}_{12}$ the shear rate, and $G_r(t)$ is the shear relaxation modulus. The integration is carried out over all past times s up to the current time t. The shear relaxation modulus G_r needs to be determined to describe the transient interaction between the shear stress and shear strain at various loading rates.

The relaxation modulus can be determined in several ways. Fourier sine and cosine transformations relate this relaxation modulus to the storage and loss moduli [7], respectively. Such conversions can be performed if the dynamic moduli can be described with relatively simple functions of frequency, which consequently allows for analytical evaluation of the inverse sine or cosine transforms. Such an example has been shown by Campanella and Peleg [61] for visco-elastic liquids. The material considered here showed a response that corresponds more to a visco-elastic solid and therefore the presence of an equilibrium modulus G_∞ must be accounted for. Moreover, such conversions assume that the dynamic moduli are known through the entire frequency domain, whereas only three to four orders of frequency are generally available from experiments. It is hard to estimate the errors introduced due to this assumption.

Another way to apply a conversion was thoroughly described by Schwarzl and Struik [62] and Schwarzl [63]. Applying a finite difference scheme for several points ω_i results in an approximation of the relaxation function G_r at the corresponding times $t_i = 1/\omega_i$. It was assumed that the measured dynamic moduli are available at a uniformly spaced grid of logarithmic frequencies. The ratio between successive frequencies is assumed to be a factor of two. The proposed approximation for the relaxation modulus reads:

$$G_r(t) \simeq G'_L(\omega) - \sum_k c_k G''_L(2^k\omega) - \sum_k d_k\{G'_L(2^{k+1}\omega) - G'_L(2^k\omega)\} \tag{45}$$

The equilibrium modulus G_∞ is implicitly accounted for in the $G'(\omega)$ terms. Several sets of constants c_k and d_k were supplied [63] to yield an approximation for G_r, together with an estimation of the maximum error introduced. All schemes were evaluated, but minor differences were observed in the determined relaxation functions. Moreover, the estimated errors are much smaller than the standard deviations of G'_L and G''_L for the sample of five specimens tested here. The following scheme was selected:

$$G_r(t) \simeq G'_L(\omega) - 0.528G''_L(\omega/2) + 0.112G''_L(\omega) + 0.0383G''_L(2\omega) \quad \text{with } t = 1/\omega \tag{46}$$

The scheme (46) was applied to the data represented with the filled markers in Fig. 25 and resulted in the $G(t_i)$ points as shown in Fig. 26. A continuous function is favourable to evaluate transient responses with Eq. (44). The grey line in Fig. 26 shows the exponential fit with coefficients a and b, and a constant representing the equilibrium modulus G_∞.

Consider a piece of material that behaves according to the approximated relaxation function G_r, and which is free of stresses initially at $s = 0$. By applying an instantaneous constant shear rate $\dot{\gamma}_{12}$, Eq. (44) can be further developed as:

$$\begin{aligned}\sigma_{12}(t) &= \dot{\gamma}_{12}\int_{s=0}^{t} G_r(t-s)\mathrm{d}s \\ &\approx \dot{\gamma}_{12}\int_{s=0}^{t} a(t-s)^{-b}\mathrm{d}s + \dot{\gamma}_{12}G_\infty t \\ &= \dot{\gamma}_{12}\left(G_\infty t - \frac{a}{b-1}t^{1-b}\right) \quad \text{for } \begin{matrix} b>1 \\ b<1 \end{matrix}\end{aligned} \tag{47}$$

Fig. 27 shows these stress responses for three different shear strain rates $\dot{\gamma}_{12}$, which are typically in the order as they appear during the stamp forming process. The material shows a close to elastic response, however, slightly dependent on shear rate.

9. Conclusions

Available methods for longitudinal intra-ply shear characterisation of UD fibre reinforced melts have been reviewed, their shortcomings have been identified, and the torsion bar method has subsequently been introduced. Small strain dynamic testing can be utilised to perform a thorough rheological characterisation of the material. The kinematics of the torsionally loaded bar and the relations to determine its shear property were outlined. Sensitivity analyses showed that most reliable shear property measurements can be obtained by using specimens with a close to square cross section. The specimen dimensions must further be tailored to the available space in the aimed fixtures and the measurement device to be used.

The torsion bar method was subsequently implemented in practise and critically evaluated. The conditions that lead to linear and non-linear material behaviour have been explored for UD/PEEK with a 60% fibre volume fraction at a temperature of

390 °C. Dynamic moduli from linear visco-elasticity theory were determined. Non-linear material responses were observed for relatively small shear strain amplitudes. This was concluded from the distorted waveform data recorded during frequency sweeps carried out at various strain amplitudes. Further analyses were focussed on linear small strain frequency sweeps. The dynamic moduli were obtained with standard deviations of 20–30%. A consistently larger storage modulus indicates predominantly elastic behaviour at small strains. Moreover, the moduli were independent of temperature in this small strain regime. The behaviour is attributed to the presence of multiple fibre–fibre interactions. Both storage and loss moduli weakly depend on frequency. These characteristics are representative for a visco-elastic solid or a weak gel.

The method shows good potential to become a standard test in the future, considering the relatively small effort to perform the experiments, the nowadays easily accessible standard rheometers, and the repeatability of the data obtained.

10. Recommendations

Future work is recommended to be focussed on further validation and, where possible, improvement of this characterisation test by round-robin benchmarking. A logical next step is to apply the torsion bar method extensively in the large strain regime. As an example, the torque can be measured while subjecting the specimen to an instantaneously applied constant rotation rate until a given maximum rotation angle has been reached. Fig. 28 shows the typical response for two rotation rates and two temperatures, which were obtained for a torsion bar specimen of $11 \times 13 \times 61$ mm. Research on this topic is encouraged, but one must be aware of the following issues:

- The relations for shear strain in Eq. (20) were developed by assuming small displacements, which is not the case for the large rotations in Fig. 28.
- Fibre tensioning and bending effects are expected to affect the response in the large strain regime.
- The large strain regime is likely to be accompanied with non-linear material behaviour. A correct stress–strain relationship can be established by applying parameter identification methods, by which the material property data are determined that lead to the best approximation of the measured torque/rotation response.
- Slip in the grips could lead to a significant influence of the responses when large strains are applied. The resulting shearing deformation could therefore deviate from the employed relationship (such as (20)), which derives the shearing distribution from the imposed rotation angle. Analyses of slip and specimen deformation are highly recommended, but these are hard to measure due to the poor accessibility of the specimen at high temperatures. Integrated camera systems for rheometers become increasingly available, which may open up possibilities to analyse the specimen deformations during testing.

Acknowledgements

This project is funded by the ThermoPlastic composites Research Center (TPRC). The support of the Region Twente and the Gelderland & Overijssel team for the TPRC, by means of the GO Programme EFRO 2007–2013, is also gratefully acknowledged.

References

[1] Gutowski TG. Resin flow/fiber deformation model for composites. SAMPE Quart 1985;16(4):58–64.
[2] Schlimbach J, Mitschang P. Process-based cycle time estimation for the thermoplastic tape placement. J Thermoplast Compos Mater 2006;19(5):507–29.
[3] Cogswell FN. The experience of thermoplastic structural composites during processing. Compos Manuf 1991;2(3–4):208–16.
[4] Cogswell FN. Flow and rheology in polymer composites manufacturing. Elsevier Science B.V.; 1994. pp. 127–202 [chapter Continuous-Fibre Systems].
[5] Murtagh AM, Mallon PJ. Composite sheet forming, composite materials series, vol. 11. Elsevier Science B.V.; 1997. pp. 163–216 [chapter Characterisation of Shearing and Frictional Behaviour during Sheet Forming].
[6] Ó Brádaigh CM. Flow and rheology in polymer composites manufacturing. Elsevier Science B.V.; 1994. pp. 517–69 [chapter Sheet Forming of Composite Materials].
[7] Ferry JD. Viscoelastic properties of polymers. 3rd ed. John Wiley & Sons; 1980.
[8] Pipes RB, Coffin DW, Simacek P, Shuler SF, Okine RK. Flow and rheology in polymer composites manufacturing. Elsevier Science B.V.; 1994. pp. 85–202 [chapter Rheological Behavior of Collimated Fiber Thermoplastic Composite Materials].
[9] Spencer AJM. Continuum theory of the mechanics of fibre – reinforced composites. Springer Verlag; 1984 [chapter Constitutive theory for strongly anisotropic solids].
[10] Rogers TG. Rheological characterization of anisotropic materials. Composites 1989;20(1):21–7.
[11] Beaussart AJ, Hearle JWS, Pipes RB. Constitutive relationships for anisotropic viscous materials. Compos Sci Technol 1993;49(4):335–9.
[12] Christensen RM. Effective viscous flow properties for fiber suspensions under concentrated conditions. J Rheol 1993;37(1):103–20.
[13] Tarnopol'skii YM, Kintsis TY. Methods for testing composites in shear (review). Mech Compos Mater 1981;17(3):364–76.
[14] Lee S, Munro M. Evaluation of in-plane shear test methods for advanced composite materials by the decision analysis technique. Composites 1986;17(1):13–22.
[15] Harrison P, Clifford MJ. Design and manufacture of textile composites. Cambridge, UK: Woodhead Publishing Ltd.; 2005 [chapter Rheological Behaviour of Pre-impregnated Textile Composites].
[16] Haanappel SP, ten Thije R, Akkerman R. Forming predictions of UD reinforced thermoplastic laminates. In 14th European conference on composite materials, ECCM 2010; 2010.
[17] Groves DJ. A characterization of shear flow in continuous fibre thermoplastic laminates. Composites 1989;20(1):28–32.
[18] Groves DJ, Stocks DM. Rheology of thermoplastic–carbon fibre composite in the elastic and viscoelastic states. Compos Manuf 1991;2(3–4):179–84.
[19] Groves DJ, Bellamy AM, Stocks DM. Anisotropic rheology of continuous fibre thermoplastic composites. Composites 1992;23(2):75–80.
[20] Benbow JJ, Cogswell FN, Cross MM. On the dynamic response of viscoelastic fluids. Rheol Acta 1976;15(5):231–7.
[21] Scobbo Jr JJ, Nakajima N. Dynamic mechanical analysis of molten thermoplastic/continuous graphite fiber composites in simple shear deformation. In National SAMPE technical conference, vol. 21; 1989. p. 730–43.
[22] Scobbo Jr JJ, Nakajima N. Modification of the mechanical energy resolver for high temperature and rigid material applications. Polym Test 1990;9(4):245–55.
[23] Wheeler AB, Jones RS. A characterization of anisotropic shear flow in continuous fibre composite materials. Compos Manuf 1991;2(3–4):192–6.
[24] Jones RS, Roberts RW. Anisotropic shear flow in continuous fibre composites. Composites 1994;25(3):171–6.
[25] Roberts RW, Jones RS. Rheological characterization of continuous fibre composites in oscillatory shear flow. Compos Manuf 1995;6(3–4):161–7.
[26] McGuinness GB, Ó Brádaigh CM. Characterisation of thermoplastic composite melts in rhombus-shear: the picture-frame experiment. Compos Part A: Appl Sci Manuf 1998;29(1–2):115–32.
[27] Stanley WF, Mallon PJ. Intraply shear characterisation of a fibre reinforced thermoplastic composite. Compos Part A: Appl Sci Manuf 2006;37:939–48.
[28] Goshawk JA, Jones RS. Structure reorganization during the rheological characterization of continuous fibre-reinforced composites in plane shear. Compos Part A: Appl Sci Manuf 1996;27:279–86.
[29] Cao J, Akkerman R, Boisse P, Chen J, Cheng HS, de Graaf EF, et al. Characterization of mechanical behavior of woven fabrics: experimental methods and benchmark results. Compos Part A: Appl Sci Manuf 2008;39(6):1037–53.
[30] Potter K. Bias extension measurements on cross-plied unidirectional prepreg. Compos Part A: Appl Sci Manuf 2002;33(1):63–73.
[31] Potter K. In-plane and out-of-plane deformation properties of unidirectional preimpregnated reinforcement. Compos Part A: Appl Sci Manuf 2002;33(11):1469–77.
[32] Larberg YR, Akermo M. In-plane properties of cross-plied unidirectional prepreg. In ICCM international conferences on composite materials; 2007.
[33] Advani SG, Creasy TS, Shuler SF. Composite sheet forming. Composite materials series, vol. 11. Elsevier Science B.V.; 1997.
[34] Dykes RJ, Martin TA, Bhattacharyya D. Determination of longitudinal and transverse shear behaviour of continuous fibre-reinforced composites from vee-bending. Compos Part A: Appl Sci Manuf 1998;29(1–2):39–49.
[35] Timoshenko SP, Goodier JN. Theory of elasticity. 3rd ed. McGraw-Hill; 1970.
[36] Demakos CB. Stress fields induced in fibre-reinforced composite laminate beams by torsion. Compos Sci Technol 2002;62(2):213–22.

[37] Nederveen CJ, van der Wal CW. A torsion pendulum for the determination of shear modulus and damping around 1 Hz. Rheol Acta 1967;6(4):316–23.
[38] Nederveen CJ, Tilstra JF. Clamping corrections for torsional stiffness of prismatic bars. J Phys D: Appl Phys 1971;4(11):1661–7.
[39] Saint-Venant B. Memoires des Savants Etrangers 14; 1855. p. 233–560 [chapter Memoire sur la torsion des prismes].
[40] Szabó I. Höhere technische mechanik. Berlin: Springer Verlag; 1960.
[41] Akkerman R. Euler–Lagrange simulations of nonisothermal viscoelastic flows. Ph.D. thesis, University of Twente; 1993.
[42] Huétink J. On anisotropy, objectivity and invariancy in finite thermo-mechanical deformations. In 9th ESAFORM conference on material forming; 2006. p. 355–8.
[43] ten Thije RHW. Finite element simulations of laminated composite forming processes. Ph.D. thesis, University of Twente; 2007.
[44] Haanappel SP, ten Thije RHW, Sachs U, Rietman AD, Akkerman R. In-plane shear characterisation of uni-directionally reinforced thermoplastic melts. In: Menary G, editor. AIP conference proceedings, the 14th international ESAFORM conference on material forming, vol. 1353. American Institute of Physics; 2011. p. 930–5.
[45] ASTM. Standard test method for plastics: dynamic mechanical properties: in torsion. Annual Book of ASTM Standards, 08.03: D 5279 01.
[46] Mark JE, editor. Polymer data handbook. Oxford University Press Inc.; 1999.
[47] Day M, Sally D, Wiles DM. Thermal degradation of poly(aryl-ether-ether-ketone). Experimental evaluation of crosslinking reactions. J Appl Polym Sci 1990;40(9–10):1615–25.
[48] Nguyen QD, Boger DV. Measuring the flow properties of yield stress fluids. Ann Rev Fluid Mech 1992;24(1):47–88.
[49] de Bruijne DW, Pritchard NJ, Papenhuijzen JMP. Constitutive equations applied to dispersed systems. Rheol Acta 1974;13(3):418–23.
[50] Mewis J, Spaull AJB. Rheology of concentrated dispersions. Adv Colloid Interface Sci 1976;6(3):173–200.
[51] Hyun K, Wilhelm M, Klein CO, Cho KS, Nam JG, Ahn KH, et al. A review of nonlinear oscillatory shear tests: analysis and application of large amplitude oscillatory shear (LAOS). Prog Polym Sci (Oxford) 2011;36(12):1697–753.
[52] Cox WP, Merz EH. Correlation of dynamic and steady flow viscosities. J Polym Sci 1958;28:619.
[53] Onogi S, Matsumoto T, Warashina Y. Rheological properties of dispersions of spherical particles in polymer solutions. Trans Soc Rheol 1973;17(1):175–90.
[54] Khan MA, Mitschang P, Schledjewski R. Identification of some optimal parameters to achieve higher laminate quality through tape placement process. Adv Polym Technol 2010;29(2):98–111.
[55] Reiner M. The deborah number. Phys Today 1964;17(1):62.
[56] Citerne GP, Carreau PJ, Moan M. Rheological properties of peanut butter. Rheol Acta 2001;40(1):86–96.
[57] Stickel JJ, Knutsen JS, Liberatore MW, Luu W, Bousfield DW, Klingenberg DJ, et al. Rheology measurements of a biomass slurry: an inter-laboratory study. Rheol Acta 2009;48(9):1005–15.
[58] Moreira R, Chenlo F, Torres MD. Effect of sodium chloride, sucrose and chestnut starch on rheological properties of chestnut flour doughs. Food Hydrocolloids 2011;25(5):1041–50.
[59] Shen F, Tay TE, Li JZ, Nigen S, Lee PVS, Chan HK. Modified Bilston nonlinear viscoelastic model for finite element head injury studies. J Biomech Eng 2006;128(5):797–801.
[60] Kitano T, Kataoka T, Nagatsuka Y. Dynamic flow properties of vinylon fibre and glass fiber reinforced polyethylene melts. Rheol Acta 1984;23(4):408–16.
[61] Campanella OH, Peleg M. On the relationship between the dynamic viscosity and the relaxation modulus of viscoelastic liquids. J Rheol 1987;31(6):511–3.
[62] Schwarzl FR, Struik LCE. Analysis of relaxation measurements. Adv Mol Relax Process 1968;1(3):201–55.
[63] Schwarzl FR. Numerical calculation of stress relaxation modulus from dynamic data for linear viscoelastic materials. Rheol Acta 1975;14(7):581–90.